frontiers | Frontiers in Environmental Science

TYPE Review
PUBLISHED 12 June 2023
DOI 10.3389/fenvs.2023.1212355

OPEN ACCESS

EDITED BY
Xiaofei Tan,
Hunan University, China

REVIEWED BY
Zacharias Frontistis,
University of Western Macedonia, Greece
Jing Zou,
Huaqiao University, China
Shaohua Wu,
Guangdong University of Petrochemical Technology, China

*CORRESPONDENCE
Wenchao Peng,
wenchao.peng@tju.edu.cn

RECEIVED 28 April 2023
ACCEPTED 30 May 2023
PUBLISHED 12 June 2023

CITATION
Sun Y, Liu J, Fan X, Li Y and Peng W (2023), Synthesis and application of iron sulfide–based materials to activate persulfates for wastewater remediation: a review.
Front. Environ. Sci. 11:1212355.
doi: 10.3389/fenvs.2023.1212355

Synthesis and application of iron sulfide–based materials to activate persulfates for wastewater remediation: a review

Yuqing Sun[1], Jiapeng Liu[2], Xiaobin Fan[1,3], Yang Li[1,3] and Wenchao Peng[1,3]*

[1]School of Chemical Engineering and Technology, Tianjin University, Tianjin, China, [2]School of Chemical Engineering, Hebei University of Technology, Tianjin, China, [3]Zhejiang Institute of Tianjin University, Shaoxing, Zhejiang, China

Rapid industrial development has led to excessive levels of various contaminants in natural water, which poses a challenge to the innovation of environmental remediation technology. In recent years, iron sulfide and its modified materials have attracted extensive attention in environmental remediation due to their high activity in advanced oxidation processes and widespread existence in anoxic environment. This paper reviewed the latest advances of the synthesis methods for iron sulfide and modified FeS. In addition, the application of persulfate activation by iron sulfide materials (FeS, FeS_x, S–ZVI, FeS@Carbon materials and MFe_xS_y) for contaminants remediation is also reviewed, and the enhancement of this system by photo irradiation, ultrasound, and microwave have also been concluded. Additionally, the interaction mechanism of iron sulfide and persulfate with contaminants was reviewed. Based on the above contents, we concluded that the long–term stability of iron sulfide, the toxicity to organisms of iron sulfide materials in the treated water, and the combination of FeS/PS with other assisted technologies should be focused in future.

KEYWORDS

iron sulfide, water remediation, persulfate, catalytic mechanisms, synthesis

1 Introduction

As one of the global environmental problems, water pollution caused by various organic pollutants (such as drugs and metabolites, endocrine disrupting chemicals (EDCs), dyes, plastic additives, pesticides, antibiotics, etc.) is increasingly serious (Petrie, et al., 2015; Pan, et al., 2018; Li, et al., 2019a; Liu, et al., 2019; Bhatt, et al., 2021; Wang, et al., 2021). Advanced oxidation processes based on persulfates (PS–AOPs) can degrade refractory contaminants effectively via radical or non–radical routes, the related reactive oxidation species (ROSs) include $SO_4^{\bullet-}$, •OH, $O_2^{\bullet-}$, $^1O_2$, high valent metals, and electron–transfer process.

Various methods such as ultrasonic (Hao, et al., 2014), thermal (Qi, et al., 2014; Wang and Wang, 2018), electric (Silveira, et al., 2017), photo irradiation (Lin and Wu, 2014) and transition metal (Anipsitakis and Dionysiou, 2004; Wu, et al., 2022) activation have been developed to activate persulfates for pollutant degradation, among which Fe–based catalysts have wider application due to their high reactivity, stability, low cost, environmentally friendly, and simple synthesis (Li, et al., 2021a; Hou, et al., 2021; Liu, et al., 2022a).

As a rate–limiting step in Fe–mediated PS–AOPs, the low regeneration rate from Fe (III) to Fe (II) (0.002–0.01 M^{-1} s^{-1}) decrease the efficiency of the catalytic reaction (Wang, et al., 2014). Therefore, many strategies have been proposed to accelerate Fe (III)/Fe (II) cycling, such as combining bimetals or adding some reductants (Hou, et al., 2016; Luo, et al., 2020; Xiang, et al., 2020; Zhang, et al., 2022). However, the synthesis of those composite materials is complex and expensive. Therefore, catalyst with auto–enhanced effect may be more promising (Cai, et al., 2022a).

Iron sulfide (FeS), also known as mackinawite, is a kind of tetragonal system common non–toxic mineral (Gong, et al., 2016). With unique molecular structure and surface chemistry, FeS is very effective in fixing divalent metals such as Fe^{2+}, Mn^{2+}, Ca^{2+}, Mg^{2+}, Ni^{2+}, Cd^{2+} and Hg^{2+} (Wharton et al., 2000; Mariëtte, et al., 2003). Due to the reducibility of FeS, both Fe (II) and S (–II) can act as electron donors. Therefore, both surface–bound Fe (II) and self–released dissolved Fe^{2+} in FeS can serve as continuous iron sources, which can be used to activate persulfate to generate free radicals (Eqs.1, 2) (Fan, et al., 2018a). In addition, the lattice S (–II) on FeS surface can also provide electrons to Fe (III), which can effectively alleviate the excessive consumption of Fe^{2+} and accumulation of Fe^{3+} to maintain the Fe (III)/Fe (II) cycle on the catalyst surface (Eq. 3) (Hou, et al., 2022). Therefore, FeS have been used in recent years to activate PS for the degradation of organic pollutants (Sühnholz, et al., 2021; Xiang, et al., 2022).

$$\equiv Fe^{2+}/Fe^{2+} + S_2O_8^{2-} \rightarrow \equiv Fe^{3+}/Fe^{3+} + SO_4^{\bullet-} + SO_4^{2-} \quad (1)$$

$$\equiv Fe^{2+}/Fe^{2+} + HSO_5^- + H^+ \rightarrow \equiv Fe^{3+}/Fe^{3+} + SO_4^{\bullet-} + H_2O \quad (2)$$

$$S^{2-} + 2Fe^{3+} \rightarrow S^0 + 2Fe^{2+} \quad (3)$$

The purpose of this paper is to focus on the synthesis, modification, and application of iron sulfide to activate PS for pollutants degradation in recent years. Specifically, this review aims to: 1) review the synthesis methods of iron sulfide particles; 2) Clarify the activation mechanism of iron sulfides for PMS to degrade organic pollutants; and 3) Put forward the existing knowledge gap in exist research and the prospect of future research.

2 Synthesis methods of iron sulfide

2.1 The synthesis of FeS and other FeS_x

FeS particles are usually synthesized by physicochemical and biochemical methods. Physicochemical method is the co–precipitation of different types of iron salts and sulfide salts in the aqueous solution under the condition of hypoxia (Eq. 4). Common source of Fe^{2+} include ferrous chloride ($FeCl_2$), ferric sulfate heptahydrate ($FeSO_4·7H_2O$), and ammonium ferrous sulfate ($Fe(NH_4)_2·(SO_4)_2·6H_2O$). Sodium sulfide ($Na_2S$) is usually used as the source of S^{2-} (Chen, et al., 2019).

$$Fe^{2+} + S^{2-} \rightarrow FeS \quad (4)$$

Biosynthetic FeS has much attracted attention due to its environmental friendliness. In general, ferroreductive bacteria (FRBS) and sulfate–reducing bacteria (SRBS) reduce Fe^{3+} and sulfur substances (including sulfate, thiosulfate and elemental sulfur) to S^{2-} and Fe^{2+} respectively, and subsequently to produce FeS nanoparticles (Xie, et al., 2013; Zhou, et al., 2017).

However, FeS particles prepared by traditional methods, especially co–precipitation, tend to rapidly aggregate, which greatly reduces their specific surface area and leads to significant reduction in pollutant removal efficiency (Gong, et al., 2012). Therefore, the preparation of dispersible FeS nanoparticles with small particle size, large specific surface area and high reactivity has attracted extensive attention. Previous studies have explored various techniques to prepare FeS nanoparticles with controllable particle morphology and size distribution, such as reverse micelles (Ajay, et al., 1996), SRB–assisted production (Watson, et al., 2001), high–energy mechanical grinding (Soori, et al., 2016), wet chemical synthesis (Paknikar, et al., 2005), etc.

Recent studies have shown that the presence of polymer stabilizers and surfactants during the synthesis of FeS particles can effectively control the nucleation and growth of nanoparticles through simultaneous electrostatic repulsion and steric hindrance, thus effectively promoting the size control of FeS in aqueous solution. This can not only reduce the aggregation of nanostructured materials, but provide a large number of functional groups to degrade pollutants (Shao, et al., 2016). For example, polyelectrolyte stabilizer carboxymethyl cellulose (CMC) is widely used to modify nanoparticles to enhance the stability of nano FeS due to a large number of carboxylic and hydroxyl groups in its macromolecular chains (Xiong, et al., 2009; Gong, et al., 2012; Gong, et al., 2014; Van Koetsem, 2016). Additionally, other macromolecular biomaterials with similar physical and chemical properties, such as starch, cyclodextrin (CD), chitosan, polysaccharide sodium alginate (SA), etc., have also been used as stabilizers to synthesize nano FeS particles (Shao, et al., 2016; Wu, et al., 2017; Sun, et al., 2018a; Sun, et al., 2018b). The mechanism and processes of synthesis of iron sulfide are exhibited in Figures 1A, B.

In aqueous solution, the reducibility of ferrous ions will decrease with the pH value decreasing, which means acidic environment can inhibit the oxidation of ferrous ions to ferric ions (Liu, et al., 2022b). Therefore, the elemental valence state of the synthesized iron sulfide catalysts can also be adjusted. Liu et al. (Liu, et al., 2022a) obtained three kinds of iron sulfides by controlling the pH of the co–precipitation system of iron and sulfide salt to synthesize FeS_2, Fe_7S_8, Fe_3S_4 at pH = 3, 5, 7, respectively. Hydrothermal method is also a common method for the synthesis of FeS_x. To mix dissolved ferrous salts ($FeSO_4·7H_2O$, $FeCl_2·4H_2O$, etc.) with sulfide (thiourea, $Na_2S_2O_3$, etc.) in a reaction vessel, and keep the vessel at 200°C for 24 h to obtain FeS_2 (Wang, et al., 2020a; Mohamed, et al., 2023). Magnetic Fe_3S_4 was obtained by dissolving $FeCl_3·6H_2O$ and thiourea in ethylene glycol, and then heating in a hydrothermal kettle at 180°C for 12 h (Shi, et al., 2020; Li, et al., 2022b). The mechanism and processes of synthesis of FeSx are exhibited in Figure 1C

Because of the synergistic effect between zero–valent iron (ZVI) and Fe_xS_y (FeS and FeS_2), S–ZVI has high reactivity and selectivity for PS activation to degrade refractory contaminants (Li, et al., 2017a; Wei, et al., 2022). S–ZVI can be synthesized by the "one–pot" process, where ferrous ions react with borohydrides and sulfides. While in the two–step process, sulfur compounds (sodium sulfide and thiosulfate) are added to the synthesized nZVI to form S–ZVI (Li, et al., 2017b). For S–ZVI prepared by one–pot process, FeS_x are

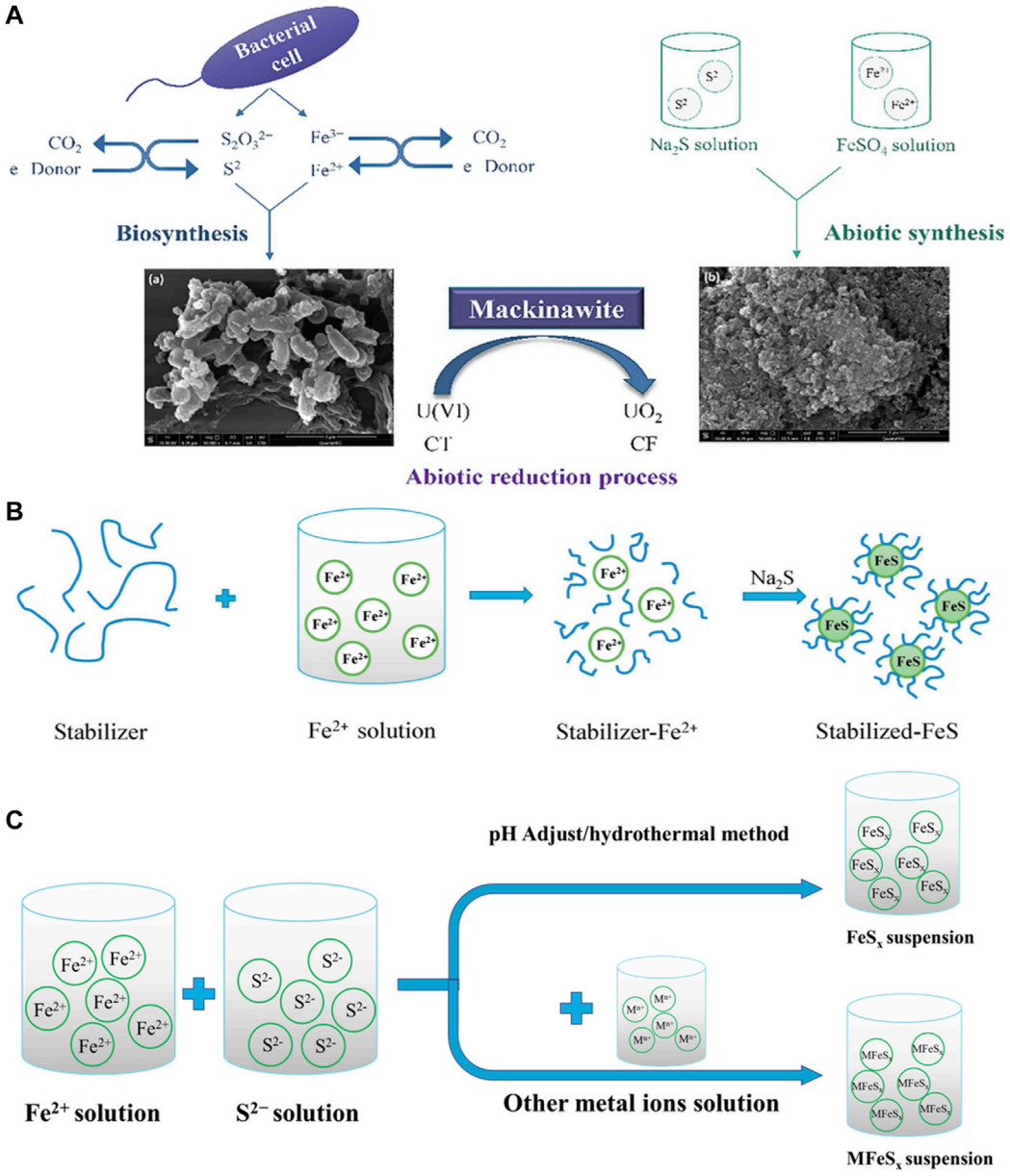

FIGURE 1
(A) The mechanism of biological and abiotic synthesis of FeS. **(B)** The modified methods of nano–sized FeS particles by coating stabilizers. Adapted with permission from (Chen et al., 2019). Copyright 2019 Elsevier. **(C)** The mechanism of synthesis of FeSx and multicomponent iron sulfide.

distributed both inside and on the surface of ZVI particles, while prepared by two–step method, FeS_x are only formed on the surface of ZVI to form a core–shell structure (Su, et al., 2018; Xu, et al., 2019). In addition, vulcanized micro–scale S–ZVI can be prepared by ball–milling S and ZVI powders under dry conditions (Gu, et al., 2017; He, et al., 2022). The structure, physicochemical properties and performance in PS based Fenton–like reactions of S–ZVI produced by various synthesis methods are mainly affected by the molar ratio of S/Fe (Fan, et al., 2017; Zhang, et al., 2020). Kim et al. (Kim, et al., 2011) reported that the degradation rate of TCE by S–nZVI increased linearly with increasing molar ratio of S/Fe, but decreased with increasing molar ratio of S/Fe when the concentration of $Na_2S_2O_4$ increased to 2.0 g/L (S/Fe molar ratio was 0.33). However, Han et al. (Han and Yan, 2016) reported that when S/Fe ratio is smaller than 0.025, the degradation rate of TCE becomes faster with the increase of S/Fe molar ratio, and then becomes stable when the molar ratio of S/Fe molar ratio exceeds 0.025. Rajajayavel et al. (Rajajayavel and Ghoshal, 2015) showed that the reducing ability of S–nZVI on TCE was strongly dependent on the S/Fe molar ratio, which provided the highest TCE dechlorination rate in the range of 0.04–0.083. Since the reaction conditions (including synthesis methods, reaction conditions and the properties of the target stain, etc.) used by different researchers to obtain the optimal S/Fe molar ratio are very different, the optimal S/Fe molar ratio values in different studies are not comparable. Based on the above examples, higher S/Fe molar ratio results in more

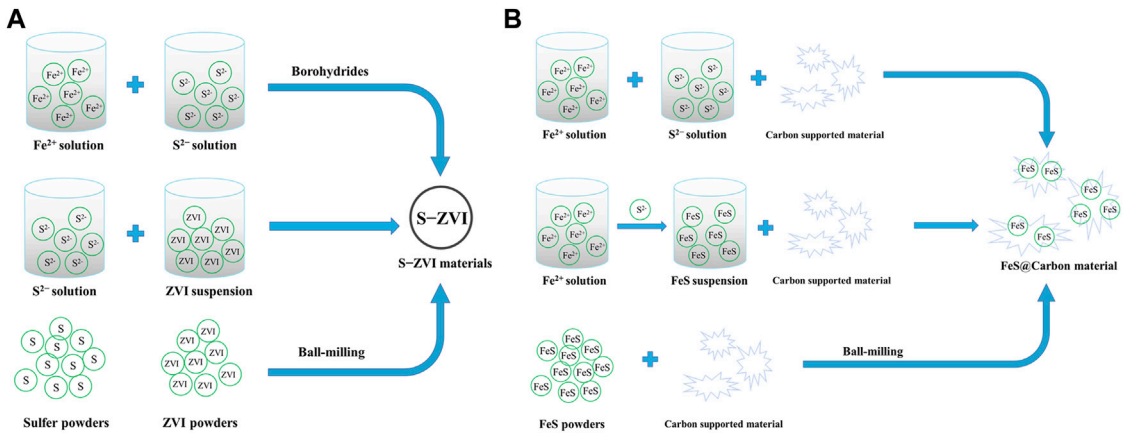

FIGURE 2
(A) The mechanism synthesis of S–ZVI. **(B)** The mechanism synthesis of Fe@Carbon materials.

production of FeSx and a larger surface area of the synthesized S–ZVI, thus facilitates the pollutants degradation (Gu, et al., 2017; Huang, et al., 2017). However, excess S content blocks the active Fe site on the surface, which will decrease their activity for PS activation. In addition, the conversion of Fe^0 to ferric/ferrous (hydrogen) oxides may be intensified at high S/Fe ratio, leading to waste of ZVI with strong reducing capacity (Li, et al., 2017a). Therefore, it is essential to find the optimal S/Fe molar ratio in different reaction systems. The mechanism and processes of synthesis of S–ZVI are exhibited in Figure 2A.

2.2 The synthesis of carbon modified FeS

The large surface area of carbon material can greatly reduce the agglomeration of iron–based nanoparticles, thus improving the activity of catalyst. Additionally, strong electron transfer capacity of carbon material can greatly enhance the electron transfer rate of iron–based catalyst (Li, et al., 2018; Ma, et al., 2021). Due to environmentally friendly, good surface physical and chemical properties, and rich oxygen–containing functional groups. Biochar (BC), graphene/graphene oxide (GO)/reductive graphene oxide (rGO), carbon nanotubes (CNTs), graphite carbon nitride ($g–C_3N_4$), etc., are commonly selected as supports to load FeS. They have been proven to significantly reduce the aggregation of FeS, resulting in better catalytic activity (Ma, et al., 2015; Sun, et al., 2020; Lyu, et al., 2018a; Zhang, et al., 2019a; Bin, et al., 2020; Zhuang, et al., 2020; Han, et al., 2022; Xu, et al., 2022). Generally, the composite of FeS and carbon materials can be obtained by loading iron salt on carbon materials firstly followed with sulfidation process, and freeze–drying, ultrasound or mechanical stirring are widely used loading methods (Sun, et al., 2020; Han, et al., 2022; Xu, et al., 2022). Specifically, these hybrids can be synthesized by mixing carbon materials with ferrous salt and sulfide and then reacted at high temperature under hypoxia condition (Ma, et al., 2015; Lyu, et al., 2018b; Hong, et al., 2021), or carbon materials mixed with pre–synthesized iron sulfide and then treated by hydrothermal method (Li, et al., 2022a). In addition, ball–milling can also achieve the combination of FeS with some carbon materials (Lyu, et al., 2018b; He, et al., 2021; Xia, et al., 2022). The mechanism and processes of synthesis of FeS@Carbon materials are exhibited in Figure 2B.

2.3 The synthesis of multicomponent iron sulfide

Multicomponent iron sulfides exhibit better electrochemical and catalytic properties due to the synergistic effect between metal ions and redox reactions. It can be synthesized by improved hydrothermal methods. Li et al. (Li, et al., 2020) mixed $FeCl_2$, $Co(NO_3)_2$, NH_4F and $g–C_3N_4$ powders at 25°C for 30 min, then heated the mixture in hydrothermal reactor at 140°C for 9 h. Put the Fe–Co precursor and thionoacetamide solution in hydrothermal reactor at 160°C for 6 h, $FeCo_2S_4$–CN composite can then be obtained. Nie et al. (Nie, et al., 2019) mixed CuCl, $FeCl_3·6H_2O$ and $(NH_4)_2S$ for 30 min, and heated at 200°C for 10 h in hydrothermal reactor to obtain $CuFeS_2$ NPs. Yan et al. (Yan, et al., 2020) loaded ferric nitrate, cobalt nitrate hexahydrate, ammonium fluoride, urea solution, and reduced graphene oxide film (RGOF) in a hydrothermal kettle at 120°C for 8 h, and then placed the obtained Fe–Co precursor and sodium sulfide solution in the hydrothermal reactor at 160°C for 8 h to obtain $FeCo_2S_4$/RGOF composite material. The mechanism and processes of synthesis of multicomponent iron sulfide are exhibited in Figure 1C.

3 Applications and mechanism of iron sulfides in AOPs

3.1 Bare FeS

Among various iron sulfides, FeS and FeS_2 are the most commonly used materials for persulfate activation. Since FeS is widely distributed in anoxic environment, and has strong reducibility and high reactivity to organic pollutants, it has been

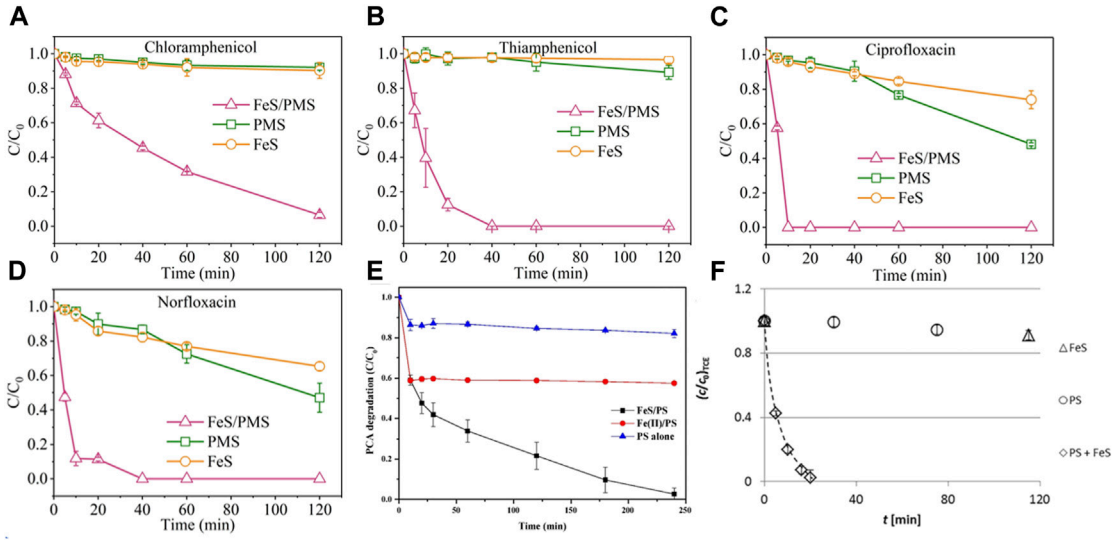

FIGURE 3
Degradation of four antibiotics in the FeS/PMS, PMS and FeS systems **(A)** CAP **(B)** TAP **(C)** CIP **(D)** NOR. Conditions $[Contaminants]_0$ = 30 μM $[PMS]_0$ = 6 mM $[FeS]_0$ = 0.6 g/L, initial *pH* = 7.0. Adapted with permission from (Xu and Sheng, 2021). Copyright 2021 Elsevier. **(E)** PCA degradation in FeS/PS system. Conditions $[PCA]_0$ = 0.2 mM $[PS]_0$ = 4 mM $[FeS]_0$ = 0.35 g/L [Fe (II)]$_0$ = 29 mg/L. Adapted with permission from (Fan, et al., 2018a). Copyright 2018 Elsevier. **(F)** Decrease in TCE concentration during the oxidation by peroxydisulfate activated with FeS. Conditions $[TCE]_0$ = 150 μM $[PS]_0$ = 6 mM $[FeS]_0$ = 3 mM, initial *pH* = 3. Adapted with permission from (Sühnholz, et al., 2020). Copyright 2020 Elsevier.

widely used as PS activators for water remediation. As shown in Figure 3, Xu et al. (Xu and Sheng, 2021) used FeS/PMS system to degrade chloramphenicol (CAP), sulfoxamycin (TAP), ciprofloxacin (CIP) and norfloxacin (NOR), and 100% NOR, 100% CIP, 93.5% CAP and 98.5% TAP was degraded within 2 h. Fan et al. (Fan, et al., 2018b) used FeS/PDS system to degrade PCA, and PCA degradation reached nearly 100% in acidic conditions within 240 min. And Sarah et al. used FeS as PDS activator and reached nearly complete removal of TCE within 20 min. These results showed that the FeS/PS system can effectively remediate the organic pollutants containing wastewater. In addition, the catalytic performance of iron–based catalysts in PS based Fenton–like reactions is summarized in Table 1.

So far, the mechanism of PS activation through FeS has been considered to be homogeneous and heterogeneous activation. Homogeneous activation refers to the continuous release of dissolved Fe^{2+} by FeS for persulfate activation, and the slow release of Fe^{2+} by FeS can effectively inhibit the self–quenching effect on $SO_4^{\bullet-}$ to promote the degradation of pollutants (Eqs. 5, 6). Heterogeneous activation refers to the surface of FeS combines Fe (II) or structural ≡Fe (II) for persulfate activation (Yuan, et al., 2015; Chen, et al., 2017; Fan, et al., 2018a; Sühnholz, et al., 2022). Fan et al. (Fan, et al., 2018b) found the presence of binding free radicals ($\equiv SO_4^{\bullet-}$) on the surface of the catalyst through radical quenching experiments, indicating the activation of persulfate by structural Fe (II). In addition, it was found that S_{aq}^{2-} ion itself could not activate PS to produce oxidation radicals (Eq. 7) (Oh, et al., 2011), but SO_4^{2-}, S^0, polysulfide (S_n^{2-}) and S^- were detected on the surface of FeS after PS activation by X–ray photoelectron spectroscopy (XPS) and FT–IR analysis (Eq. 3 and Eqs. 8, 9), indicating that S (–II) in FeS can indirectly provide electrons to PS by facilitating the reduction of Fe (III) to Fe (II). Once S^{2-} is exhausted, Fe (II) regeneration via PS reduction will dominate, since S^{2-} is non–renewable in FeS/PS systems (Eq. 10). In addition, Xu et al. (Xu and Sheng, 2021) also demonstrated that Fe (IV) was generated in the FeS/PS system, but its contribution to pollutant degradation as reactive species is not significant.

$$SO_4^{\bullet-} + HSO_5^- \rightarrow SO_5^{\bullet-} + SO_4^{2-} + H^+ \quad (5)$$

$$SO_4^{\bullet-} + SO_4^{\bullet-} \rightarrow S_2O_8^{2-} \quad (6)$$

$$S^{2-} + S_2O_8^{2-} \rightarrow 9SO_4^{2-} \quad (7)$$

$$(n-1)S^0 + HS^- \rightarrow S_n^{2-} + H^+ \; (n = 2-6) \quad (8)$$

$$S_n^{2-} + FeS \rightarrow S_{n-1}^{2-} + FeS_2 \quad (9)$$

$$Fe^{3+} + HSO_5^- \rightarrow Fe^{2+} + SO_5^{\bullet-} + H^+ \quad (10)$$

Therefore, the mechanism of FeS for persulfate activation can be proposed in Figures 4A, B, which is also explained as follows:

Homogeneous activation process: Firstly, FeS release Fe^{2+} ions (Eqs. 11, 12), which can activate PS to form $SO_4^{\bullet-}$ (Eqs. 1, 2). The Fe^{3+} can be reduced to Fe^{2+} by reacting with FeS or S^{2-} (Eq. 3, 13). Finally, the regenerated Fe^{2+} continue to maintain PS activation for pollutant degradation.

Heterogeneous activation process: ≡Fe (II) in FeS activates PS as electron donor to produce $SO_4^{\bullet-}$(Eqs. 1, 2), then $\equiv S^{2-}$ and HS^- adsorbed on the surface of FeS can also give electrons to ≡Fe (III) and reduce it to ≡Fe (II), ensuring that the heterogeneous activation process can be continued (Eqs. 14, 15) (Yang, et al., 2022).

$$FeS + H_2O \rightarrow Fe^{2+} + HS^- + OH^- \quad (11)$$

$$FeS + H^+ \rightarrow Fe^{2+} + HS^- \quad (12)$$

$$FeS + 8Fe^{3+} + 4H_2O \rightarrow 9Fe^{2+} + SO_4^{2-} + 8H^+ \quad (13)$$

$$2 \equiv Fe^{3+} + HS^- \rightarrow 2 \equiv Fe^{2+} + S^0 + H^+ \quad (14)$$

$$\equiv Fe^{3+} + S^{2-} \rightarrow \equiv Fe^{2+} + S^0 \quad (15)$$

TABLE 1 Summary of the reported work on the activation of persulfates by Fe–based catalysts for the removal of target pollutant.

Catalyst	Target pollutant	Oxidant	Condition	Removal efficiency	Mechanism	Ref
$FeSO_4$	Aniline (AN)	PDS	T = 25°C; [$Na_2S_2O_8$] = 8 mM; [AN] = 0.1 mM; [$FeSO_4$] = 2 mM; Reaction time = 8 min	97.73%	$SO_4^{\bullet-}$	Yan, et al. (2021)
$FeSO_4$	Trichloroethylene (TCE)	PS	T = 20°C ± 0.5°C; [TCE] = 0.15 mM; [PS] = 2.25 mM; [$FeSO_4$] = 0.3 mM; Reaction time = 30 min	100%	$SO_4^{\bullet-}$, •OH, $O_2^{\bullet-}$	Wu, et al. (2015)
$FeSO_4$	Diatrizoate (DTZ)	PS	[DTZ] = 5 mg/L; [PS] = 10 mM; [$FeSO_4$] = 0.1 mM; Reaction time = 120 min	69%	$SO_4^{\bullet-}$, •OH	Shang, et al. (2019)
nZVI	Sulfamethazine (SMT)	PS/H_2O_2	[PS] = 1 mM; [H_2O_2] = 0.5 mM; [ZVI] = 2 mM; [SMT] = 50 mg/L; *pH* = 6.8; Reaction time = 30 min	96%	$SO_4^{\bullet-}$, •OH	Wu, et al. (2020a)
nZVI	Chloramphenicol (CAP)	PMS	[PMS] = 0.2 mM; [CAP] = 10 mg/L; [nZVI] = 0.5 g/L; *pH* = 7; Reaction time = 120 min	95.2%	$SO_4^{\bullet-}$, •OH	Tan, et al. (2018)
mZVI	1,1,1–trichloroethane (TCA)	PDS	T = 20°C; [PDS] = 9.0 mM; [ZVI] = 2.08 g/L; [TCA] = 0.15mM; Reaction time = 720 min	97%	$SO_4^{\bullet-}$, •OH	Gu, et al. (2015)
nZVI/BC	Nonylphenol (NP)	PDS	T = 25 °C; [PDS] = 5 mM; [nZVI/BC_3] = 0.4 g/L; [NP] = 20 mg/L; *pH* = 7 Reaction time = 120 min	96.2%	$SO_4^{\bullet-}$, •OH	Hussain, et al. (2017)
Fe@GBC	17β–Estradiol (E2)	PDS	[PDS] = 400 mg/L; [Fe@GBC] = 40 mg/L; [E2] = 6 mg/L; *pH* = 6; Reaction time = 90 min	100%	$SO_4^{\bullet-}$, •OH	Zhang, et al. (2019b)
Fe@AC	2,4–dinitrotoluene (2,4–DNT)	PDS	T = 15°C; [PDS] = 100 mg/L; [Fe] = 300 mg; [AC] = 100 mg; [2,4–DNT] = 100 mg/L; *pH* = 7; Reaction time = 340 min	94%	$SO_4^{\bullet-}$	Ma, et al. (2017)
NZVI/zeolite	Acid orange 7 (AO7)	PMS	*pH* = 3.0; [PMS] = 0.2 mM; [AO7] = 8.4 mg/L; [z–nZVI] = 0.1 g/L; Reaction time = 40 min	100%	$SO_4^{\bullet-}$, •OH, $O_2^{\bullet-}$	Fu, et al. (2020)
Iron–based MOF (MIL–88–A)	Naproxen (NPX)	PDS	[*PS* = 5 mM; [NPX] = 50 mg/L; [MIL–88–A] = 125 mg/L; *Ph* = 6.48; UVA irradiation = 450 μW cm^{-2}; Reaction time = 180 min	100%	$SO_4^{\bullet-}$, •OH	El Asmar, et al. (2021)
Fe–N/C	Bisphenol F (BPF)	PMS	T = 30°C; [PMS] = 1.0 Mm; [Fe–N/C] = 50.0 mg/L; [BPF] = 10.0 mg/L; *pH* 7.0; Reaction time = 90 min	97.1%	$SO_4^{\bullet-}$, •OH, $^1O_2$	Wu, et al. (2020b)
Fe–N/C	Bisphenol A (BPA)	PMS	T = 30°C; [PMS] = 0.5 mM; [Fe–N/C] = 100.0 mg/L; [BPA] = 10.0 mg/L; *pH* = 7.0; Reaction time = 90 min	96.4%	$^1O_2$, high–valent iron–oxo species (HV–Fe–O)	Wang, et al. (2023a)
Fe@C–PDA	Tetracycline (TC)	PDS	[PDS] = 0.20 g/L; [Fe@C–PDA] = 0.20 g/L; [TC] = 100 mg/L; *pH* = 7.0; Reaction time = 60 min	99.7%	$SO_4^{\bullet-}$, •OH	Zhu, et al. (2019)
Fe_3O_4	Acetaminophen (APAP)	PMS	[PMS] = 0.2 mM; [Fe_3O_4 MNPs] = 0.8 g/L; [APAP] = 10 mg/L; Reaction time = 120 min	74.7%	$SO_4^{\bullet-}$, •OH	Tan, et al. (2014)
α–Fe_2O_3	Rhodamine B (Rh B)	PDS	[PDS] = 10 mM; [α–Fe_2O_3] = 0.3 g/L; [Rh B] = 20 mg/L; Initial *pH* = 6.7; Reaction time = 30 min	100%	$SO_4^{\bullet-}$, •OH	Meng, et al. (2020)
FeOOH	Acid orange 7 (AO7)	PMS	T = 25°C ± 1 °C; [PMS]: [AO7] (mol) = 20: 1; [FeOOH] = 0.3 g/L; *pH* = 5; Reaction time = 30 min	91.4% (δ–FeOOH); 42% (α–FeOOH); 24.9% (β–FeOOH); 29.5% (γ–FeOOH)	$SO_4^{\bullet-}$, $O_2^{\bullet-}$	Fan, et al. (2018b)

(Continued on following page)

TABLE 1 (*Continued*) **Summary of the reported work on the activation of persulfates by Fe–based catalysts for the removal of target pollutant.**

Catalyst	Target pollutant	Oxidant	Condition	Removal efficiency	Mechanism	Ref
FeS	Chloramphenicol (CAP); Thiamphenicol (TAP); Ciprofloxacin (CIP); Norfloxacin (NOR)	PMS	T = 25°C; *pH* = 7; [PMS] = 6 mM; [Organics] = 30 μM; [FeS] = 0.6 g/L; Reaction time = 120 min	93.5% (CAP); 98.5% (TAP); 100% (CIP); 100% (NOR)	$SO_4^{\bullet-}$, •OH, Fe (IV)	Xu and Sheng (2021)
Pyrite (FeS_2)	Atrazine (ATR)	PS	*PS* = 3 Mm; [FeS_2] = 4.2 mM; [ATR] = 20 mg/L; *pH* = 7.0	100%	$SO_4^{\bullet-}$, •OH	Wang, et al. (2020b)
S–mFe^0	Sulfamethoxazole (SMX)	PMS	[PMS] = 0.3 mM; S/Fe = 0.1 (molar ratio), T = 30°C, [S–mFe^0] = 0.15 g/L; [SMX] = 10 mg/L; Reaction time = 15 min	89.8%	$SO_4^{\bullet-}$, •OH	Li, et al. (2019b)
S–nZVI	Sulfamethazine (SMT)	PDS	[PDS] = 1 mM; [S–nZVI] = 56 mg/L; [Fe/S] = 20; [SMT] = 40 mg/L; *pH* = 3.0; Reaction time = 60 min	100%	$SO_4^{\bullet-}$, •OH	Dong, et al. (2019b)
$CoFe_2O_4$	Triphenyl phosphate (TPhP)	PMS	T = 25°C; [PMS] = 0.2 Mm; [$CoFe_2O_4$] = 0.25 g/L; [TPhP] = 10μM; *pH* = 7.0; Reaction time = 90 min	78%	$SO_4^{\bullet-}$, •OH, $SO_5^{\bullet-}$	Song, et al. (2019)
$CuFe_2O_4$	p–nitrophenol (PNP)	PDS	[PDS] = 8 mM; [$CuFe_2O_4$] = 30 g/L; [PNP] = 50 mg/L; [pH] = 7.0; Reaction time = 60 min	89%	$SO_4^{\bullet-}$, •OH	Li, et al. (2017a)
MFe_2O_4 (M = Co, Cu, Mn, and Zn)	Di–n–butyl phthalate (DBP)	PMS	[PMS] = 20 μM; [MFe_2O_4] = 0.1 g/L; [DBP] = 20 μM; *pH* = 7.0; Reaction time = 30 min	81% ($CoFe_2O_4$); 62.3% ($CuFe_2O_4$); 42.3% ($MnFe_2O_4$); 30.0% ($ZnFe_2O_4$)	$SO_4^{\bullet-}$, •OH	Ren, et al. (2015)

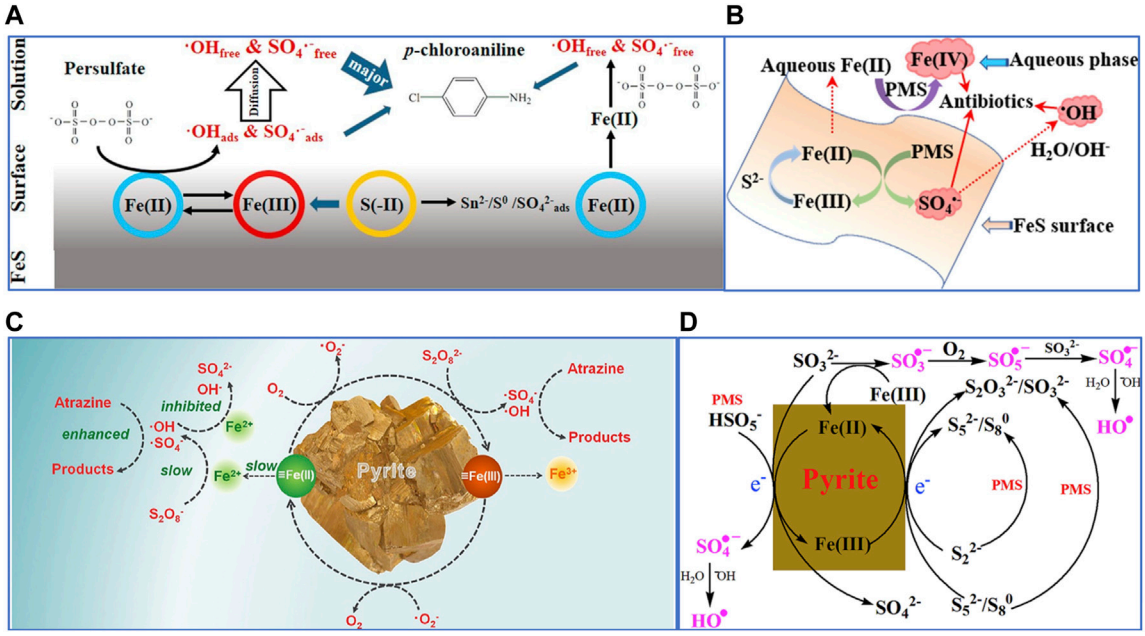

FIGURE 4
(A) The catalytic mechanism of mackinawite/PDS system. Adapted with permission from (Fan, et al., 2018a). Copyright 2018 Elsevier. **(B)** The possible mechanism of reactive species generation in the FeS/PMS system. Adapted with permission from (Xu and Sheng, 2021). Copyright 2021 Elsevier. **(C)** Degradation mechanism of atrazine by pyrite/PS. Adapted with permission from (Wang, et al., 2020c). Copyright 2020 Elsevier. **(D)** Proposed pathways of PMS activation by pyrite. Adapted with permission from (Zhou, et al., 2018). Copyright 2018 Elsevier.

In addition, it is worth mentioning that solution pH is one of the most significant influencing factors in the remediation of contaminants by nano–sized FeS, which not only plays an important role in the decomposition of oxidants, but affects the surface charge of FeS–based catalysts and the speciation of substrates to be transformed (Chen, et al., 2019; Li, et al., 2021b).

In general, when the solution pH is greater than the pH value at point of zero charge (pH_{pzc}), the surface of the catalyst is negatively charged, otherwise positively charged (Li, et al., 2020). Under strongly alkaline or strongly acidic conditions, the adsorption capacity is significantly reduced, which not only destroys the active sites on surface and accelerates the corrosion of FeS nanoparticles, but promotes the hydrolysis of bio−modifiers, thus decrease the stability and dispersion of modified nano−FeS. In addition, under strongly alkaline conditions, Fe (II) species will be reduced due to the precipitation of ferric hydroxide in reaction system and produce passivation layer on the surface of FeS. Additionally, negatively charged hydroxide ions compete for absorption with other negatively charged contaminants, which will influence the degradation of contaminants by FeS. Therefore, neutral conditions can provide optimal degradation of pollutants with FeS materials as catalysts for PS.

3.2 FeS_x

FeS_2 can also effectively activate persulfate to degrade pollutants, and the good persulfate activation performance is attributed to the low−valent Fe and S (Fe^{2+} and S^{-1}) (Hou, et al., 2021). By being fully oxidized to SO_4^{2-} and Fe^{3+}, FeS_2 can provide 15 electrons. Therefore, FeS_2 can slowly and sustainably releases dissolved Fe^{2+}, which activates persulfates to produce reactive free radicals to degrade pollutants (Eqs. 1, 2). Fe^{2+} comes from the water corrosion process of FeS_2 (Oh, et al., 2011), and Fe^{2+} will activate persulfate to be consumed, which will accelerate the water corrosion reaction of FeS_2 (Eq. 10 and Eqs. 16–18). $\equiv S^{-1}$ could also give electrons to persulfate or Fe (III), which would cause Fe^{2+} to continue to form (Liang, et al., 2010). In addition, surface−bound ≡Fe (II) can activate molecular oxygen to produce $O_2^{\bullet-}$ through single electron transfer pathway (Liu, et al., 2015), while surface−bound ≡Fe (II) is also reduced, allowing the degradation to continue. The mechanism of FeS_2 for persulfate activation can be proposed in Figures 4C, D.

$$\mathbf{FeS_2 + H_2O \rightarrow S^0 + Fe^{2+} + HS^- + OH^-} \quad (16)$$

$$\mathbf{FeS_2 + 2S_2O_8^{2-} \rightarrow Fe^{2+} + 2SO_4^{\bullet-} + 2SO_4^{2-} + 2S^0} \quad (17)$$

$$\mathbf{FeS_2 + 14Fe^{3+} + 8H_2O \rightarrow 15Fe^{2+} + 2SO_4^{2-} + 16H^+} \quad (18)$$

S−ZVI has been widely used in activating persulfate to degrade refractory organic pollutants, such as tetracycline (Dong, et al., 2019a), bisphenol S (Cai and Zhang, 2022), tetrabromobisphenol A (Quoc, et al., 2021), trichloroethylene (Zhou, et al., 2021a), sulfadiazine (SDZ) (Guo, et al., 2020), etc., indicating that S−ZVI/PS system can effectively treat organic wastewater.

S−ZVI has high electron utilization efficiency, 10–50 times larger than that of unsulfide ZVI. Its sulfide layer can significantly enhance the activity of ZVI and promote to release ferrous ions into the environment (Fan, et al., 2016; Fan, et al., 2018b). This is because there are delocalized electrons in the FeS layer, which has good electrical conductivity and facilitates the transfer of electrons from Fe^0, thus accelerating the ferrous ions formation (Kim, et al., 2011; Song, et al., 2017). According to electrochemical test, the results of Tafel curve and electrochemical impedance spectroscopy (EIS) also confirm that S−ZVI supports better electron transfer (Turcio−Ortega, et al., 2012; Wang, et al., 2019). Hence, the sulfide layer mainly acts as conductor of electrons to promote the release of Fe^{2+} during the reaction process, rather than source of Fe^{2+} production, which can be used to activate persulfate.

In addition to promoting the release of ferrous ions, the sulfur compounds in the sulfide layer have strong reducing capacity, which can reduce Fe^{3+} to Fe^{2+} (Eq. 3), and these ferrous species will be subsequently used to activate persulfate based on the electron transfer capacity of the sulfide layer (Fan, et al., 2018a; Li, et al., 2019a). Fe^0 in S−ZVI can also reduce Fe (III) to Fe (II) (Eq. 19), and a small amount of FeS_2 in S−ZVI can react with water to produce Fe^{2+} to further enhancing the iron cycle (Eq. 20). The cycle of iron species enables the degradation reaction to be carried out contumely and efficiently (Liu, et al., 2015). The mechanism of S−ZVI for persulfate activation can be proposed in Figure 5.

$$\mathbf{Fe^0 + 2 \equiv Fe - S - Fe^{3+} \rightarrow Fe^{2+} + 2 \equiv Fe - S - Fe^{2+}} \quad (19)$$

$$\mathbf{2FeS_2 + 7O_2 + H_2O \rightarrow 2FeSO_4 + 2H_2SO_4} \quad (20)$$

3.3 Carbon modified FeS

FeS@Caobon materials has been widely used to activate persulfate for degradation of organic pollutants, such as petroleum hydrocarbons (Xia, et al., 2022), 2, 4−dichlorophenoxyacetic acid (Hong, et al., 2021), tetracycline (He, et al., 2021), sulfamethazine (Jin, et al., 2022), etc., indicating the potential of FeS@Caobon/PMS system in wastewater remediation.

It has been reported that in heterogeneous activation systems, radicals are first produced near the surface of the activator and then diffused into the solution to degrade pollutants (Liu, et al., 2014), but it has also been reported that both activation and degradation processes may occur near the surface of the carbon−based activator (He, et al., 2019). By measuring the levels of dissolved ion (dissolved Fe^{2+} and total Fe) in the reaction system, and using hydrophobic phenol and 1, 10−phenanthroline to chelate with surface−bound Fe (II) and dissolved Fe^{2+} as quenchers, confirming that the active radicals were mainly generated on the Fe@Carbon surface (He, et al., 2021; Han, et al., 2022). According to the XPS results of catalysts before and after the reaction, the ratio of Fe^{2+} to S^{2-} decreased significantly after the reaction, while that of other sulfur species such as S_n^{2-} and SO_4^{2-} increased, indicating that Fe (II) and S (−II) species were involved in the reaction process, and S (−II) contribute to the conversion of Fe (III) and Fe (II), which will further enhance the activation of PS (Xia, et al., 2022; Yu, et al., 2022). All of these results suggest that surface−bound Fe (II) plays an important role in the PS activation process and generates ROSs on the FeS@Carbon surface. In addition, a small amount of Fe^{2+} dissolved in solution can also directly activate persulfate to produce free radicals (He, et al., 2021).

During the process of contaminants degradation in FeS@Carbon/PS system, carbon materials can prevent the agglomeration of FeS particles to make FeS particles evenly dispersed, which increase the chance of catalyst contact with solution and further increase the concentration of sustainably released Fe^{2+} (Wang, et al., 2017). Besides, the adsorption

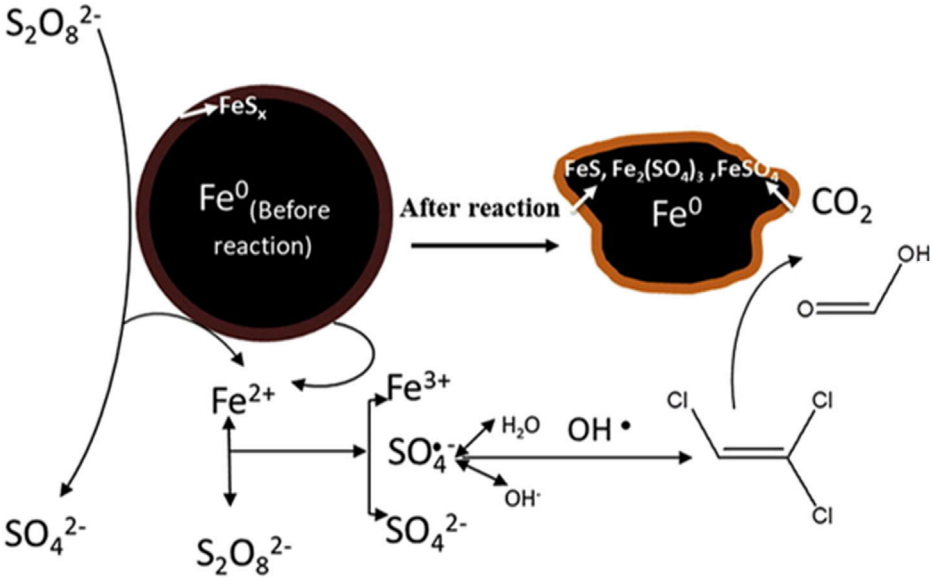

FIGURE 5
Possible degradation mechanism of TCE in S–ZVI/PS system. Adapted with permission from (Dong, et al., 2019a). Copyright 2019 Elsevier.

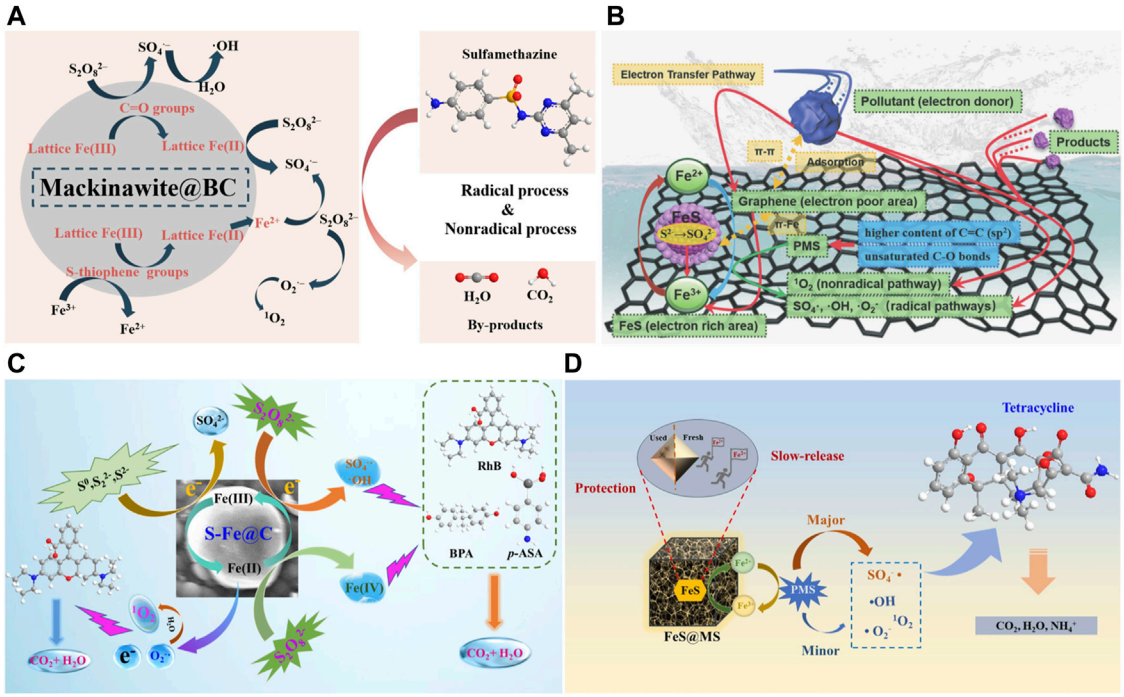

FIGURE 6
(A) Possible degradation mechanism of sulfadimethacil (SMT) in FeS@BC/PS system. Adapted with permission from (Jin, et al., 2022). Copyright 2022 Elsevier. **(B)** Mechanism of tetracycline removal by an FeS/graphene–based catalyst (DMG). Adapted with permission from (Zhuang, et al., 2020). Copyright 2020 Royal Society of Chemistry. **(C)** Proposed mechanism for various contaminants degradation in the S–Fe@C/PDS system. Adapted with permission from (Yu, et al., 2022). Copyright 2022 Elsevier. **(D)** Possible mechanism of peroxymonosulfate activation by FeS@MS for TC degradation. Adapted with permission from (Han, et al., 2022). Copyright 2022 Elsevier.

capacity of carbon materials can make contaminants adsorbed on the surface or inside of composite materials, which make the free radicals produced easier to contact with contaminants (Qu, et al., 2022). Additionally, carbon material itself can act as intermediary of electron transport to accelerate the electron transfer process and improve the degradation efficiency (Qiu, et al., 2021), CNTs and BC

has strong electron donor groups on surface, such as hydrogen peroxide (−OOH) and hydroxyl (−OH), which can also activate persulfate to produce more radicals (Eqs. 21–24) (Zhou, et al., 2020; Qiu, et al., 2022). In the composite of FeS and graphene, the bond length between FeS and graphene layer is relatively long, which indicates the weaker bonding, resulting in the higher activity of S to react with SO_5^{2-} during PMS activation. With long bond length, greater electron localization could be facilitated on the S sites to reduce the barrier of pollutant bonding and accelerate the regeneration of metal species (Zhuang, et al., 2020).

Therefore, there are three possible mechanisms of FeS@Carbon to activate persulfate: 1) the adsorption of contaminants by FeS@Carbon; 2) The active sites on catalyst surface, such as oxygen−containing functional groups, Fe^{2+}, S^{2-}, etc. act as electron donors in reaction process to activate PS and then produce ROSs for pollutants degradation (Eqs. 21–30). In addition, S^{2-} also participates in the reduction of Fe^{3+}, enabling the continuous generation of Fe^{2+}, which can be further used for the activation of PS (Eqs. 1–3); 3) Carbon materials can accelerate the electron transfer process, which promote the electron transfer from pollutants to PS and further improve the generation rate of radicals on catalyst surface. The mechanism of FeS@Carbon for persulfate activation can be proposed in Figure 6.

$$-OOH_{surf} + S_2O_8^{2-} \rightarrow -OO\bullet_{surf} + SO_4^{\bullet-} + HSO_4^- \quad (21)$$

$$-OOH_{surf} + HSO_5^- \rightarrow -OO\bullet_{surf} + SO_4^{\bullet-} + H_2O \quad (22)$$

$$-OH_{surf} + S_2O_8^{2-} \rightarrow -O\bullet_{surf} + SO_4^{\bullet-} + HSO_4^- \quad (23)$$

$$-OH_{surf} + HSO_5^- \rightarrow -O\bullet_{surf} + SO_4^{\bullet-} + H_2O \quad (24)$$

$$SO_4^{\bullet-} + H_2O \rightarrow SO_4^{2-} + \bullet OH + H^+ \quad (25)$$

$$SO_4^{\bullet-} + OH^- \rightarrow SO_4^{2-} + \bullet OH \quad (26)$$

$$S_2O_8^{2-} + 2H_2O \rightarrow HO_2^- + 2SO_4^{2-} + 3H^+ \quad (27)$$

$$S_2O_8^{2-} + HO_2^- \rightarrow SO_4^{\bullet-} + SO_4^{2-} + H^+ + O_2^{\bullet-} \quad (28)$$

$$O_2^{\bullet-} + 2H_2O \rightarrow H_2O_2 + 2OH^- + {}^1O_2 \quad (29)$$

$$\bullet OH/SO_4^{\bullet-}/{}^1O_2 + \text{contaminants} \rightarrow \text{intermediates} \rightarrow CO_2 + H_2O \quad (30)$$

3.4 Multicomponent iron sulfide

Compared with single−component sulfide, multi−component metal sulfide exhibits better catalytic performance due to its richer redox reactions and synergistic effects between metals (Li, et al., 2019c). Moreover, as an electron donor, the low electronegativity of S^{2-} can promote the redox cycle of metal ions, making multi−component metal sulfide an effective catalyst for the activation of PMS. $CuFeS_2$ (Nie, et al., 2019), $NiFe_2S_4$ (Fan, et al., 2022), Cu_2FeSnS_4 (CFTS) (Li, et al., 2022a), $CoFe_2S_4$ (Li, et al., 2022b) etc., have been widely used in the field of persulfate activation to degrade organic pollutants, showing good pollutant removal effect.

During the process of persulfate activation by polymetallic sulfide, Cu^+, Co^{2+}, Fe^{2+}, Ni^{2+} act as active sites to accelerate the generation of radicals such as $SO_4^{\bullet-}$, •OH, $O_2^{\bullet-}$ by destroying the O−O bond of PS, and they are themselves oxidized into Ni^{3+}, Fe^{2+}, Ni^{3+}, Co^{3+}. (Eqs. 31, 32). Due to the strong reducibility of sulfur species such as S^{2-} and S_2^{2-}, the high valent metal ions formed can be reduced to low valent states (Eqs. 33–35). The reduction of Fe^{3+} by Cu^+ and Ni^{2+} is easy to achieve, which is thermodynamically advantageous (Eqs. 36, 37) (Nie, et al., 2019; Fan, et al., 2022). Therefore, the synergistic interaction between these metals on the catalyst surface facilitates interfacial electron transfer. In addition, ROSs produced by hydrolysis of persulfate can also oxidize high−valent metals to low−valent metals (Eq. 10), and the regenerated active sites such as Cu^+, Ni^{2+} and Fe^{2+} on the surface can again participate in the continuous generation of ROSs induced by persulfate activation. In the CFTS/PMS system, there is S→M σ bond ((M = Cu, Fe, and Sn) which is favorable for electron transfer and contribute to form ≡Fe (II)*. It has been reported that Sn(II) can also activate persulfate to produce active free radicals due to the synergy between ≡Fe (II)* and Sn (Eqs. 38–40) (Kong, et al., 2019). The mechanism of multicomponent iron sulfide for persulfate activation can be proposed in Figures 7A–C.

$$Fe^{2+}/Cu^+/Ni^{2+}/Co^{2+} + HSO_5^- \rightarrow Fe^{3+}/Cu^{2+}/Ni^{3+}/Co^{3+} + SO_4^{\bullet-} + OH^- \quad (31)$$

$$Fe^{2+}/Cu^+/Ni^{2+}/Co^{2+} + S_2O_8^{2-} \rightarrow Fe^{3+}/Cu^{2+}/Ni^{3+}/Co^{3+} + SO_4^{\bullet-} + SO_4^{2-} \quad (32)$$

$$2S^{2-} + Fe^{3+}/Cu^{2+}/Ni^{3+}/Co^{3+} \rightarrow Fe^{2+}/Cu^+/Ni^{2+}/Co^{2+} + S_n^{2-} \quad (33)$$

$$S_n^{2-} + Fe^{3+}/Cu^{2+}/Ni^{3+}/Co^{3+} \rightarrow Fe^{2+}/Cu^+/Ni^{2+}/Co^{2+} + S^0 \quad (34)$$

$$S^0 + Fe^{3+}/Cu^{2+}/Ni^{3+}/Co^{3+} \rightarrow Fe^{2+}/Cu^+/Ni^{2+}/Co^{2+} + SO_4^{2-} \quad (35)$$

$$\equiv Cu(I)/Cu^+ + \equiv Fe(III)/Fe^{3+} \rightarrow \equiv Fe(III)/Fe^{2+} + \equiv Cu(II)/Cu^{2+} \quad (36)$$

$$\equiv Ni(II)/Ni^{2+} + \equiv Fe(III)/Fe^{3+} \rightarrow \equiv Fe(III)/Fe^{2+} + \equiv Ni(III)/Ni^{3+} \quad (37)$$

$$Fe(II) + \equiv \overset{S\rightarrow M\sigma}{\rightarrow} S \rightarrow M\sigma \equiv Fe(II)^* \quad (38)$$

$$2 \equiv Fe(II)^* + \equiv Sn(IV) \rightarrow 2 \equiv Fe(III) + \equiv Sn(II) \quad (39)$$

$$\equiv Sn(II) + 2S_2O_8^{2-} \rightarrow \equiv Sn(IV) + 2SO_4^{\bullet-} + 2SO_4^{2-} \quad (40)$$

Considering the poor dispersion of metal sulfides and large amount of metal ions leaching, the researchers further modified these catalysts. For example, Li. et al. (Li, et al., 2020) used $FeCo_2S_4$ modified g−C_3N_4 ($FeCo_2S_4$−CN) composite for PMS activation to degrade sulfamethoxazole (SMX). As shown in Figure 7D, in this system, there is a synergistic effect between $FeCo_2S_4$ and g−C_3N_4, thus the removal rate of SMX is higher than that of $FeCo_2S_4$/PMS, g−C_3N_4/PMS and PMS alone. Moreover, due to the synergistic effect between metal ions and g−C_3N_4, iron and cobalt ions, excessive leaching of metal ions is avoided. Li. et al. (Li, et al., 2022a) synthesized $CoFe_2S_4$/BC catalyst by a two−step hydrothermal method and combined it with PMS for the degradation of sodium sulfadimethacil (SMT). As shown in Figure 7E, in this system, in addition to the free radical pathway induced by the metal active site, there is also a non−free radical pathway. On the one hand, electrons can be transferred directly from the contaminants to the PMS through the active center of BC, leading to the direct decomposition of the pollutant. On the other hand, BC can activate the O−O bond in the PMS and directly oxidize the target compound.

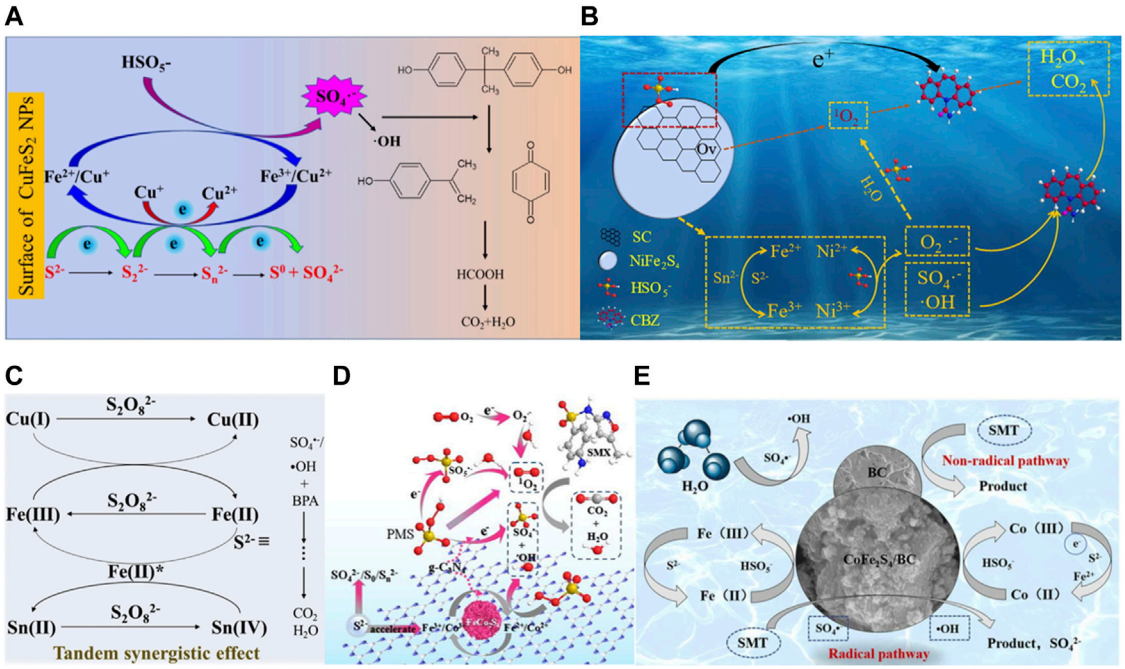

FIGURE 7
(A) Proposed catalytic mechanism for PMS activation and BPA degradation by $CuFeS_2$. Adapted with permission from (Nie, et al., 2019). Copyright 2019 Elsevier. **(B)** The mechanism of SC/$NiFe_2S_4$ activating PMS to degrade CBZ, Adapted with permission from (Fan, et al., 2022). Copyright 2022 Elsevier. **(C)** The proposed oxidation mechanism in the Cu_2FeSnS_4/PMS process, Adapted with permission from (Kong, et al., 2019). Copyright 2019 Elsevier. **(D)** The mechanism of $CoFe_2S_4$/BC activating PMS to degrade SMT. Adapted with permission from. Copyright 2020 Elsevier. **(E)** Proposed mechanism for the catalytic SMT oxidation over the $CoFe_2S_4$/BC/PMS system. Adapted with permission from (Li, et al., 2022c). Copyright 2022 Elsevier.

4 Hybrid activation systems

4.1 Photoassisted systems

FeS and its derivatives are considered promising candidates for photocatalytic water treatment due to their ability to absorb visible and/or ultraviolet light, narrow optical band gap, and charge transport properties (Ayodhya and Veerabhadram, 2018; Li, et al., 2021a). Bibhutibhushan et al. (Show, et al., 2017) synthesized FeS nanospheres by a simple electrochemical route, which act as photocatalysts to successfully degrade alizarin red S (ARS), methylene blue (MB), rose red (RB) and phenol, and no degradation of these dyes was observed in the dark and very slow degradation was observed in the absence of FeS but the presence of light, which indicates that FeS has a strong synergistic effect when working together with photoassisted technologies.

During the reaction process, when FeS are exposed to visible light, illumination causes the excitation of valence band electrons in the conduction band, and this charge separation leads to the formation of electron–hole pairs (Suroshe, et al., 2018). Photogenerated electron (e^-)–hole pairs (h^+) can react with adsorbed surface species such as O_2, H_2O, and OH^- to form ROSs such as O^{2-} and •OH, for pollutants degradation (Eqs. 41–45) (Nair, et al., 2011; Chabri, et al., 2016). In addition, the Fe^{2+} and S^{2-} in FeS can react as persulfate activator for pollutants degradation. Additionally, visible light will accelerate the cyclic conversion between Fe^{3+} and Fe^{2+} (Eq. 46) (Chen, et al., 2021), further improving the continuous degradation. Hence, possible light–induced reactions can be proposed as Eqs. 1–3 and Eqs. 41–46:

$$\mathbf{FeS + h\nu \rightarrow FeS(h^+) + e^-} \quad (41)$$

$$\mathbf{h^+ + H_2O_{2ads} \rightarrow \bullet OH + H^+} \quad (42)$$

$$\mathbf{h^+ + OH^-/OH_{ads} \rightarrow \bullet OH} \quad (43)$$

$$\mathbf{e^- + O_{2ads} \rightarrow O^{2-}} \quad (44)$$

$$\mathbf{\bullet OH / O^{2-} + contaminants \rightarrow intermediates \xrightarrow{FeS(h^+)} CO_2 + H_2O} \quad (45)$$

$$\mathbf{Fe(III)(OH)^{2+} + h\nu \rightarrow Fe^{2+} + \bullet OH} \quad (46)$$

4.2 Electro–assisted systems

Electrochemical advanced oxidation processes (EAOPs) have attracted increasing attention due to their environmental compatibility, ease of scaling up and high efficiency in degrading refractory contaminants compared to conventional advanced oxidation processes (Luo, et al., 2020). Iron sulfide shows good electrocatalytic performance due to its excellent electrical conductivity, hybrid d orbital, and general redox properties (Li, et al., 2021b), which has great potential in the field of wastewater treatment when combined with EAOPs.

Ammar. et al. (Ammar, et al., 2015) used pyrite as a heterogeneous source of Fe^{2+} catalyst to degrade tyrosol (TY) in an electro–assisted process, which possesses superior performance due to the self–regulation of Fe^{2+} content in the medium. As shown in

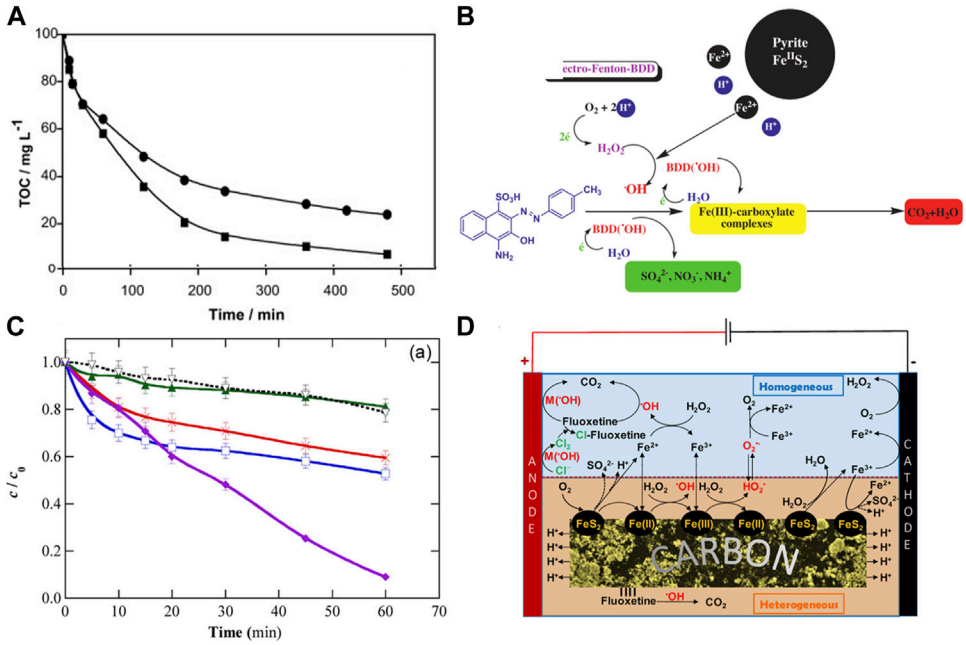

FIGURE 8
(A) Comparison between pyrite/EF system and classical EF system for evolution of TOC removal, and **(B)** The mechanism of FeS_2/EF system for AHPS degradation. Adapted with permission from (Labiadh, et al., 2015). Copyright 2015 Elsevier. **(C)** Normalized concentration decay of fluoxetine during the EF process (solutions containing 0.049 mM drug), and **(D)** the mechanism of FeS_2/C–catalyzed heterogeneous EF treatment at mild pH. Adapted with permission from (Ye, et al., 2020). Copyright 2020 American Chemical Society.

Figure 8A, (Labiadh, et al., 2015),used pyrite/EF system to generate H_2O_2 *in situ* and regenerate Fe^{2+} to completely remove azo dye (4–amino–3–hydroxy–2–p–toluene –naphthalene–1–sulfonic acid) (AHPS) from water, the mineralization rate of pyrite/EF system was superior to that of EF system alone under the same conditions, specifically, more than 90% TOC was removed in pyrite/EF within 300 min, whereas in the same reaction time only 70% TOC was removed with the conventional EF process. This is due to the self–regulation effect of pyrite on pH and soluble Fe^{2+} without additional acidification. As shown in Figure 8C, Ye et al. (Ye, et al., 2020) used FeS_2/C nanocomposites as highly active, stable and recyclable catalysts to treat fluoxetine in polyphase EF system, which achieved an impressive 90% TOC removal, while conventional EF processes produce a maximum TOC removal of 60%. The good performance of pyrite/EF system was attributed to the large amount of •OH produced by the pyrite induced Fenton reaction, which mainly attributed to the following aspects: (1) The mass transfer restriction of FeS_2 is very small, and it can act as the transfer intermediate of Fe^{2+} to participate in the homogeneous reaction to produce •OH. Meanwhile, pyrite can provide rich active sites, and ≡Fe (II) can activate H_2O_2 to produce •OH by Fe–S bond. (2) the ≡Fe (II) on the surface of FeS_2 can promote the activation of molecule O_2, thus accelerating the formation of $O_2^{\bullet-}$ (Liu, et al., 2015). In addition, the boron–doped diamond (BDD) anode used in the electro–assisted system also contributes to the generation of physical adsorption •OH in pyrite/EF system. The heterogeneous mechanism of the system is dominant because the concentration of dissolved iron is relatively low. The mechanism of electro–assisted pyrite/persulfate system for contaminants degradation can be proposed in Figures 8B, D.

4.3 Ultrasonic–assisted technology

Increasing attention has been paid to the application of ultrasonic (US) combined with advanced oxidation technology in water treatment. On the one hand, US has strong mechanical effect, which can enhance the mass transfer between interfaces, remove the passivation film on the metal surface and make the surface regenerate continuously. These properties can overcome the heterogeneous mass transfer barrier in the process of degrading organic matter, and achieve good contaminants removal effect (Xiang, et al., 2022). On the other hand, US lead to form cavitation effect, and its local high temperature and high pressure can produce •OH, $O_2^{\bullet-}$ and other ROSs (Chi, et al., 2022; Savun–Hekimoğlu, 2020; Wei, et al., 2017).

Chi et al. (Chi, et al., 2022) used US to enhance ferrous sulfide (FeS) to activate persulfate (PDS) for 2'–deoxycoformycin (DCF) degradation. US/FeS/PDS system with excellent activity presented an optimal DCF degradation efficiency (98.9%), which was 56.7, 5.81, 1.48 times than that of US, US/PDS and FeS/PDS systems (Figure 9B). Wei. et al. (Xiang, et al., 2022) demonstrated good degradation effect of carbamazepine (CBZ) by using ultrasonic–enhanced FeS/PDS system, which can remove 94.2% CBZ in 60 min, while FeS/PDS system can only remove 71.2% CBZ under same conditions (Figure 9A), confirming the synergistic enhancement effect of US and FeS contributed to the degradation of contaminants.

In ultrasonic enhanced FeS/persulfate system, US can promote the interfacial sulfur–iron electron transfer and the disintegration of passivation layer, which avoid the passivation and deactivation of FeS, and provide redox energy between S^{2-}/S_x^{2-} and Fe^{2+}/Fe^{3+} to

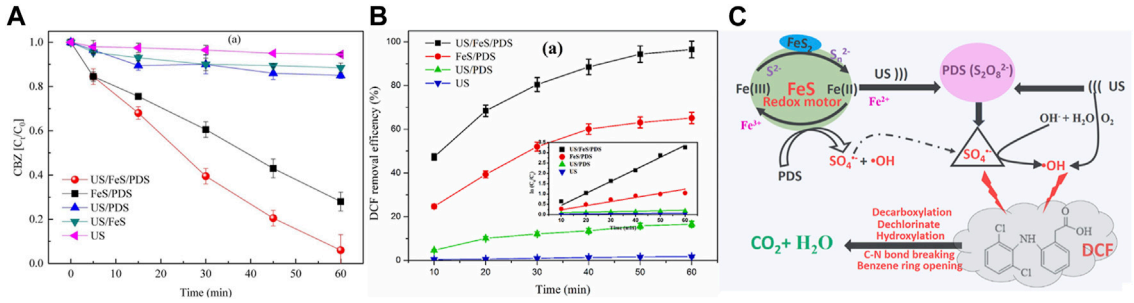

FIGURE 9
(A) Comparison of CBZ degradation during five systems. Adapted with permission from (Xiang, et al., 2022). Copyright 2022 Elsevier. **(B)**The DCF removal efficiency and kinetic constant, and **(C)** The reaction mechanism of DCF degradation in the US/FeS/PDS system. Adapted with permission from (Chi, et al., 2022). Copyright 2022 Elsevier.

promote continuous production of Fe^{2+}. Additionally, US can directly activate PDS, H_2O and dissolved oxygen to form $SO_4^{\bullet-}$ and •OH. In a word, US greatly promotes both heterogeneous and homogeneous iron cycles in the system. Hence, possible US–assisted reactions can be summarized as Eqs.1–3, Eqs. 47, 48, and the mechanism of US–assisted FeS/persulfate system for contaminants degradation can be proposed in Figure 9C

$$H_2o +))) (US) \rightarrow \bullet OH + H\bullet \quad (47)$$

$$S_2O_8^{2-} +))) (US) \rightarrow SO_4^{2-} \quad (48)$$

4.4 Microwave assisted technology

Microwave (MW) activation of persulfate has been widely studied. It has been proved to be superior to conventional thermal activation in terms of accelerating reaction rate, increasing yield and selectively activating or inhibiting reaction pathways, thus leading to higher degradation rate and significant savings in energy consumption and treatment time (Qi, et al., 2014). Wang et al. (Wang, et al., 2020a) used microwave radiation combined with FeS to activate persulfate to treat dinitrodiazophenol in explosive production wastewater. The Chemical Oxygen Demand (COD) removal efficiency of the MW–FeS/PS process reached 76.16%, which was 2.62, 2.57, and 1.42 times than that of MW/FeS, FeS/PS and MW/PS systems, indicating the strong synergistic effect between FeS and MW.

In MW–FeS/PS system, in addition to the persulfate activation performance of FeS, MW radiation can not only activate PS to produce $SO_4^{\bullet-}$ by its thermal effect, but make some functional groups and structures on organic pollutants vulnerable. Furthermore, the MW and FeS have strong synergic effect. Therefore, microwave–assisted FeS activation of persulfate can show higher treatment efficiency and higher PS utilization efficiency (Wang, et al., 2020b).

5 Reusability and stability

The reusability and stability of FeS–based catalysts are very important for their practical application. In general, FeS–based catalysts can maintain satisfactory catalytic performance in multiple continuous cycles due to the internal Fe (III)/Fe (II) cycle, which is shown in Eqs 49, 50:

$$S^{2-} + 2Fe^{3+} \rightarrow S^0 + 2Fe^{2+} \quad (49)$$

$$2S^{2-} + Fe^{3+} \rightarrow Fe^{2+} + S_n^{2-} \quad (50)$$

$$S_n^{2-} + Fe^{3+} \rightarrow Fe^{2+} + S^0 \quad (51)$$

$$S^0 + Fe^{3+} \rightarrow Fe^{2+} + SO_4^{2-} \quad (52)$$

As shown in Figure 10, the Cu_2FeSnS_4/PS system degraded more than 80% of BPA within 45 min after three reuse cycles (Yangju et al., 2019). In S–Fe@C/PDS system, no evident decline on Rh B degradation suggested the catalyst could be at least reused for five times (Yu, et al., 2022). In FeS_2/C–EF system, a slight but progressive performance decrease was observed after five cycles, with only 61% fluoxetine removal achieved at 60 min (Ye, et al., 2020). Fortunately, the activity of FeS–based catalysts can be restored by various treatments, such as washing with organic solvents (Ye, et al., 2020), ultrasonic treatment (Zhao, et al., 2020), and pickling (Peng, et al., 2020).

6 Reactive oxidation species

In the PS based Fenton–like reactions activated by FeS–based materials, organics were normally degraded through two oxidation pathways involving free radical (e.g., •OH, $SO_4^{\bullet-}$ and $O_2^{\bullet-}$) and non–radical (e.g., $^1O_2$ and Fe (IV) = O) reactive oxidation species (Li, et al., 2021b).

In general, $SO_4^{\bullet-}$ and •OH are most frequently detected radicals during PS activation. Fe (II) in the FeS–based catalysts reacts with PS and split O–O bond to form $SO_4^{\bullet-}$ (Eqs 1, 2). Fan et al. (Fan, et al., 2018a) proposed that surface–bound radicals (e.g., $\bullet OH_{ads}$ and $SO_4^{\bullet-}{}_{ads}$) produced by the combination of surface Fe (II) and PS can diffuse from the catalyst surface and convert into free radicals (e.g., $\bullet OH_{free}$ and $SO_4^{\bullet-}{}_{free}$) to degrade contaminants. In PS activation process, •OH may be generated by two main pathways, one is produced by the reaction of $SO_4^{\bullet-}$ with H_2O (Eq. 25), and the other is formed by radical conversion reaction of $SO_4^{\bullet-}$ with OH^- under neutral or alkaline conditions (Eq. 26) (Zhao, et al., 2016). It was found that the main ROSs in the activation

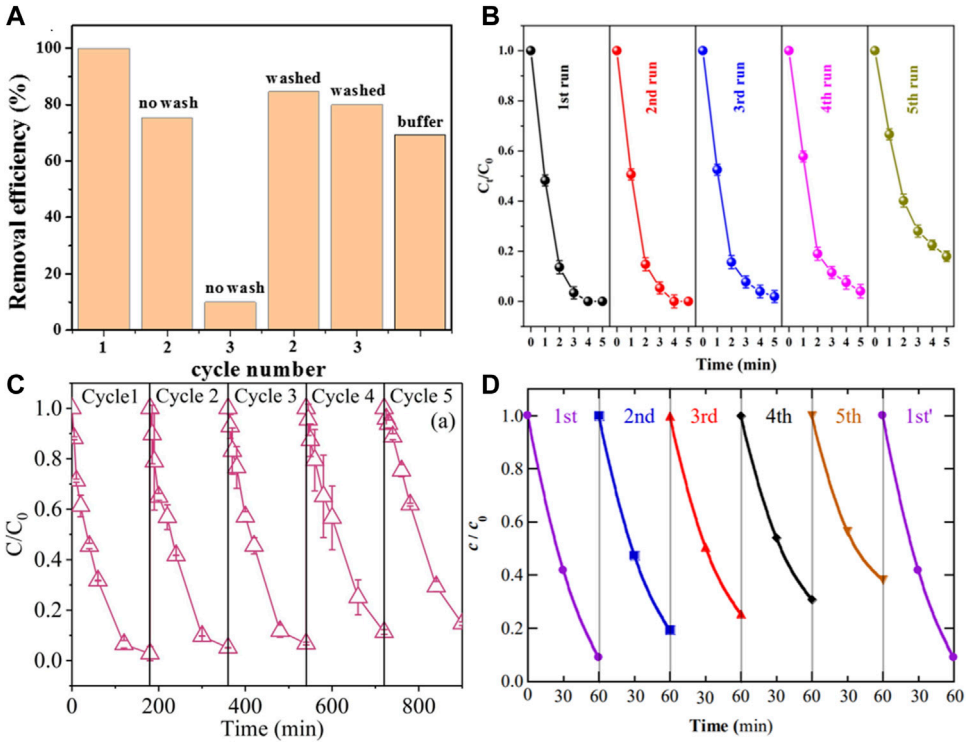

FIGURE 10
(A) Degradation of BPA by the PS/CFTS system during different activation cycles and phosphate buffer. Adapted with permission from (Kong, et al., 2019). Copyright 2019 Elsevier. **(B)** Evaluation of the stability and recyclability of S–Fe@C. Adapted with permission from (Yu, et al., 2022). Copyright 2022 Elsevier. **(C)** Catalytic activity of FeS for repeated use. Adapted with permission from (Xu and Sheng, 2021). Copyright 2021 Elsevier. **(D)** The fluoxetine concentration during the heterogeneous EF treatment with FeS_2/C nano catalyst, Cycle first′ was made once the catalyst regeneration was performed after the fifth cycle. Adapted with permission from (Ye, et al., 2020). Copyright 2020 Elsevier.

process of PS is severely pH–dependent, with $SO_4^{\bullet-}$ under acidic and •OH at alkaline conditions, respectively (Feng, et al., 2015). Usually, •OH always transform into $O_2^{\bullet-}$ under alkaline conditions through a complex series of radical chain steps (Li, et al., 2016; Ma, et al., 2019). Additionally, some FeS–based materials can also react directly with PS to produce $O_2^{\bullet-}$ (Jin, et al., 2022).

Non–radical reactive oxidation species such as $^1O_2$ and Fe (IV) = O can also be produced in the PS activation process by FeS–based materials. $^1O_2$ can be formed by the self–decomposition of PMS at alkaline condition (Eq. 53) (Zhou, et al., 2021a). Carbon modified FeS materials, such as FeS@GO and FeS@BC, can also form $^1O_2$ in PS activation, in which carbonaceous materials play a key role in the generation of $^1O_2$ (Wang, et al., 2023b). Furthermore, $^1O_2$ can result from the conversion of $O_2^{\bullet-}$ and H_2O (Eqs. 54, 55) (Zhou, et al., 2021b; Cai, et al., 2022b; Li, et al., 2022b). High–valent iron–oxo species (e.g., ≡Fe (IV) = O and ≡FeV = O) is a burgeoning ROS produced in PS activation (Li, et al., 2021a). In the activation of PS by FeS–based catalysts, the aqueous Fe (II) released from the FeS surface reacts with the PS and contribute to the formation of Fe (IV) (Eqs. 56, 57), which then effectively degrades the contaminants through non– radical pathways (Xu and Sheng, 2021).

$$\mathbf{HSO_5^- + SO_4^{2-} \rightarrow 2SO_4^{2-} + H^+ + O_2} \quad (53)$$

$$\mathbf{2O_2^{\bullet-} + 2H^+ \rightarrow H_2O + {}^1O_2} \quad (54)$$

$$\mathbf{O_2^{\bullet-} + {\bullet}OH \rightarrow OH^- + {}^1O_2} \quad (55)$$

$$\mathbf{Fe(II) + HSO_5^- \rightarrow Fe(IV) = O + SO_4^{2-} + H^+} \quad (56)$$

$$\mathbf{Fe(II) + S_2O_8^{2-} + H_2O \rightarrow Fe(IV) = O + 2SO_4^{2-} + 2H^+} \quad (57)$$

7 Toxicity assessment

To ensure safe environmental applications of FeS–based catalysts, it is necessary to conduct toxicity assessments of the catalysts and their degradation intermediates to understand the potential environmental risks to ecosystems and human health. Bare Iron sulfide (FeS) nanoparticles were reported to bind with DNA, limiting the ability of DNA to interact with other nucleic acids and amino acids (Hatton and Rickard, 2008). Rickard, D. et al. (Rickard, et al., 2011) proposed that when the concentration of FeS nanoparticles is lower than its solubility limit, it will cause incision in DNA molecules, and pose genotoxicity by reacting with polynucleic acids when above solubility limit. Furthermore, FeS particles will inhibit the growth of microorganisms and plants. For instance, in the presence of FeS nanoparticles of 2×10^{-5} M to 5×10^{-3} M, the growth rate of *E. coli* is reduced under anaerobic conditions. FeS particles may impede nutrients uptake and will decrease seed yield and viability when deposited on the roots of wild rice plants (Pastor,

et al., 2017). Zheng et al. (Zheng, et al., 2018) illustrated that exposure to CMC–FeS nanoparticles significantly damaged DNA and proteins due to nanoparticle induced oxidative stress. At present, although the biotoxicity of FeS–based catalysts in advanced oxidation processes have been gradually carried out, the evaluation of catalyst toxicity to water environment and the targeted regulation of highly toxic intermediates to harmless transformation are still insufficient.

8 Conclusion and future research expected

In the past few decades, increasing researchers have focused on the application of iron sulfides and related modified materials on water pollution. This paper reviews the synthesis of iron sulfides materials and the application of them in PS–AOPs for organic contaminant removal, and the related mechanisms were also reviewed. Although iron sulfide materials have been widely used in water pollutant restoration, there are still some knowledge gaps and challenges in its application as follows.

1) Although the modification of FeS greatly improves the activity and stability for PS activation, FeS is still easy to be oxidized in the presence of oxygen. Therefore, the long–term stability and oxidation resistance of FeS materials should be further studied to avoid the loss of reactivity of FeS, which will seriously limit its practical application in water restoration.
2) There is limited information of catalyst toxicity to water environment and the targeted regulation of highly toxic intermediates to harmless transformation, therefore, fully study the potential environmental toxicity of iron sulfide materials is essential.
3) It is necessary to combine iron sulfide with other auxiliary technologies to activate persulfate for contaminants degradation. Only a few literatures have reported the application of iron sulfide materials/PS with photo irradiation, ultrasonic, electrocatalysis, and microwave for water remediation.
4) The influence of iron sulfides on the water should be taken into account to avoid changing the physical and chemical properties and functions of the water due to the addition of iron sulfide materials.
5) A detailed and comprehensive study is needed on the whereabouts of iron sulfide materials after injection into water, especially large–scale water treatment, to ensure that there will be no secondary pollution in the process of water restoration.

Author contributions

YS: Conceptualization, Methodology, Investigation, Writing—original draft. XF: Writing—review and editing. YL: Writing—review and editing. JL: Writing—review and editing. WP: Resources, Conceptualization, Writing—review and editing, Supervision, Data curation. All authors contributed to the article and approved the submitted version.

Funding

This research was supported by the project of No. U20A20153 from the National Natural Science Foundation of China and No. 20YFZCSN00610 from the Tianjin Science and Technology Support Plan Key Projects.

Conflict of interest

The authors declare that the research was conducted in the absence of any commercial or financial relationships that could be construed as a potential conflict of interest.

Publisher's note

References

Ajay, C., Ramesh, K. S., and Charter, D. S. A., Dady, B. D. (1996). Iron sulfide catalysts for coal liquefaction prepared using a micellar technique. *Ind. Eng. Chem. Res.*, 35, 2916, 2919. doi:10.1021/ie950694y9)

Ammar, S., Oturan, M. A., Labiadh, L., Guersalli, A., Abdelhedi, R., Oturan, N., et al. (2015). Degradation of tyrosol by a novel electro–Fenton process using pyrite as heterogeneous source of iron catalyst. *Water Res.* 74, 77–87. doi:10.1016/j.watres.2015.02.006

Anipsitakis, G. P., and Dionysiou, D. D. (2004). Radical generation by the interaction of transition metals with common oxidants. *Environ. Sci. Technol.* 38 (13), 3705–3712. doi:10.1021/es035121o

Ayodhya, D., and Veerabhadram, G. (2018). A review on recent advances in photodegradation of dyes using doped and heterojunction based semiconductor metal sulfide nanostructures for environmental protection. *Mater Today Energy* 9, 83–113. doi:10.1016/j.mtener.2018.05.007

Bhatt, P., Gangola, S., Bhandari, G., Zhang, W., Maithani, D., Mishra, S., et al. (2021). New insights into the degradation of synthetic pollutants in contaminated environments. *Chemosphere* 268, 128827. doi:10.1016/j.chemosphere.2020.128827

Bin, Q., Lin, B., Zhu, K., Shen, Y., Man, Y., Wang, B., et al. (2020). Superior trichloroethylene removal from water by sulfide–modified nanoscale zero–valent iron/graphene aerogel composite. *J. Environ. Sci.* 88, 90–102. doi:10.1016/j.jes.2019.08.011

Cai, H., Zou, J., Lin, J., Li, J., Huang, Y., Zhang, S., et al. (2022a). Sodium hydroxide–enhanced acetaminophen elimination in heat/peroxymonosulfate system: Production of singlet oxygen and hydroxyl radical. *Chem. Eng. J.* 429 (2), 132438. doi:10.1016/j.cej.2021.132438

Cai, J., and Zhang, Y. (2022). Enhanced degradation of bisphenol S by persulfate activated with sulfide–modified nanoscale zero–valent iron. *Environ. Sci. Pollut. R.* 29 (6), 8281–8293. doi:10.1007/s11356-021-16156-8

Cai, Y., Fan, J., and Liu, Z. (2022b). Enhanced degradation of tetracycline over FeS–based Fenton–like process: Autocatalytic decomposition of H_2O_2 and reduction of Fe(III). *J. Hazard Mater* 436, 129092. doi:10.1016/j.jhazmat.2022.129092

Chabri, S., Dhara, A., Show, B., Adak, D., Sinha, A., and Mukherjee, N. (2016). Mesoporous CuO–ZnO p–n heterojunction based nanocomposites with high specific surface area for enhanced photocatalysis and electrochemical sensing. *Catal. Sci. Technol.* 6 (9), 3238–3252. doi:10.1039/c5cy01573a

Chen, G., Yu, Y., Liang, L., Duan, X., Li, R., Lu, X., et al. (2021). Remediation of antibiotic wastewater by coupled photocatalytic and persulfate oxidation system: A critical review. *J. Hazard Mater* 408, 124461. doi:10.1016/j.jhazmat.2020.124461

Chen, H., Zhang, Z., Feng, M., Liu, W., Wang, W., Yang, Q., et al. (2017). Degradation of 2,4–dichlorophenoxyacetic acid in water by persulfate activated with FeS (mackinawite). *Chem. Eng. J.* 313, 498–507. doi:10.1016/j.cej.2016.12.075

Chen, Y., Liang, W., Li, Y., Wu, Y., Chen, Y., Xiao, W., et al. (2019). Modification, application and reaction mechanisms of nano–sized iron sulfide particles for pollutant removal from soil and water: A review. *Chem. Eng. J.* 362, 144–159. doi:10.1016/j.cej.2018.12.175

Chi, N., Liu, J., Feng, L., Guo, Z., Chen, Y., Pan, T., et al. (2022). FeS redox power motor for PDS continuous generation of active radicals on efficient degradation and removal of diclofenac: Role of ultrasonic. *Chemosphere* 300, 134574. doi:10.1016/j.chemosphere.2022.134574

Dong, H., Hou, K., Qiao, W., Cheng, Y., Zhang, L., Wang, B., et al. (2019a). Insights into enhanced removal of TCE utilizing sulfide–modified nanoscale zero–valent iron activated persulfate. *Chem. Eng. J.* 359, 1046–1055. doi:10.1016/j.cej.2018.11.080

Dong, H., Wang, B., Li, L., Wang, Y., Ning, Q., Tian, R., et al. (2019b). Activation of persulfate and hydrogen peroxide by using sulfide–modified nanoscale zero–valent iron for oxidative degradation of sulfamethazine: A comparative study. *Sep. Purif. Technol.* 218, 113–119. doi:10.1016/j.seppur.2019.02.052

El Asmar, R., Baalbaki, A., Abou Khalil, Z., Naim, S., Bejjani, A., and Ghauch, A. (2021). Iron–based metal organic framework MIL–88–A for the degradation of naproxen in water through persulfate activation. *Chem. Eng. J.* 405, 126701. doi:10.1016/j.cej.2020.126701

Fan, D., Lan, Y., Tratnyek, P. G., Johnson, R. L., Filip, J., O Carroll, D. M., et al. (2017). Sulfidation of Iron–Based materials: A review of processes and implications for water treatment and remediation. *Environ. Sci. Technol.* 51 (22), 13070–13085. doi:10.1021/acs.est.7b04177

Fan, D., O'Brien, J. G., Tratnyek, P. G., and Johnson, R. L. (2016). Sulfidation of nano zerovalent iron (nZVI) for improved selectivity during In–Situ chemical reduction (ISCR). *Environ. Sci. Technol.* 50 (17), 9558–9565. doi:10.1021/acs.est.6b02170

Fan, J., Gu, L., Wu, D., and Liu, Z. (2018a). Mackinawite (FeS) activation of persulfate for the degradation of p–chloroaniline: Surface reaction mechanism and sulfur–mediated cycling of iron species. *Chem. Eng. J.* 333, 657–664. doi:10.1016/j.cej.2017.09.175

Fan, J., Zhao, Z., Ding, Z., and Liu, J. (2018b). Synthesis of different crystallographic FeOOH catalysts for peroxymonosulfate activation towards organic matter degradation. *Rsc Adv.* 8 (13), 7269–7279. doi:10.1039/c7ra12615h

Fan, S., Shang, J., Kulan, S., He, X., Wang, X., Nasen, B., et al. (2022). Enhanced degradation of carbamazepine in water over SC–modified NiFe2S4 nanocomposites by peroxymonosulfate activation. *Chem. Eng. J.* 450, 138190. doi:10.1016/j.cej.2022.138190

Feng, M., Qu, R., Zhang, X., Sun, P., Sui, Y., Wang, L., et al. (2015). Degradation of flumequine in aqueous solution by persulfate activated with common methods and polyhydroquinone–coated magnetite/multi–walled carbon nanotubes catalysts. *Water Res.* 85, 1–10. doi:10.1016/j.watres.2015.08.011

Fu, X., Zhang, J., Zhao, H., Zhang, S., Nie, T., Zhang, Y., et al. (2020). Enhanced peroxymonosulfate activation by coupling zeolite–supported nano–zero–valent iron with weak magnetic field. *Sep. Purif. Technol.* 230, 115886. doi:10.1016/j.seppur.2019.115886

Gong, Y., Liu, Y., Xiong, Z., Kaback, D., and Zhao, D. (2012). Immobilization of mercury in field soil and sediment using carboxymethyl cellulose stabilized iron sulfide nanoparticles. *Nanotechnology* 23 (29), 294007. doi:10.1088/0957-4484/23/29/294007

Gong, Y., Liu, Y., Xiong, Z., and Zhao, D. (2014). Immobilization of mercury by carboxymethyl cellulose stabilized iron sulfide nanoparticles: Reaction mechanisms and effects of stabilizer and water chemistry. *Environ. Sci. Technol.* 48 (7), 3986–3994. doi:10.1021/es404418a

Gong, Y., Tang, J., and Zhao, D. (2016). Application of iron sulfide particles for groundwater and soil remediation: A review. *Water Res.* 89, 309–320. doi:10.1016/j.watres.2015.11.063

Gu, X., Lu, S., Guo, X., Sima, J., Qiu, Z., and Sui, Q. (2015). Oxidation and reduction performance of 1,1,1–trichloroethane in aqueous solution by means of a combination of persulfate and zero–valent iron. *Rsc Adv.* 5 (75), 60849–60856. doi:10.1039/c5ra07655b

Gu, Y., Wang, B., He, F., Bradley, M. J., and Tratnyek, P. G. (2017). Mechanochemically sulfidated microscale zero valent iron: Pathways, kinetics, mechanism, and efficiency of trichloroethylene dechlorination. *Environ. Sci. Technol.* 51 (21), 12653–12662. doi:10.1021/acs.est.7b03604

Guo, W., Zhao, Q., Du, J., Wang, H., Li, X., and Ren, N. (2020). Enhanced removal of sulfadiazine by sulfidated ZVI activated persulfate process: Performance, mechanisms and degradation pathways. *Chem. Eng. J.* 388, 124303. doi:10.1016/j.cej.2020.124303

Han, M., Liang, L., Wang, Y., Deng, Y., Zhang, Q., Ye, Y., et al. (2022). Peroxymonosulfate activation by sponge–based FeS material for efficient degradation of tetracycline: The critical role of sponge. *J. Water Process Eng.* 46, 102605. doi:10.1016/j.jwpe.2022.102605

Han, Y., and Yan, W. (2016). Reductive dechlorination of trichloroethene by Zero–valent iron nanoparticles: Reactivity enhancement through sulfidation treatment. *Environ. Sci. Technol.* 50 (23), 12992–13001. doi:10.1021/acs.est.6b03997

Hao, F., Guo, W., Wang, A., Leng, Y., and Li, H. (2014). Intensification of sonochemical degradation of ammonium perfluorooctanoate by persulfate oxidant. *Ultrason. Sonochem* 21 (2), 554–558. doi:10.1016/j.ultsonch.2013.09.016

Hatton, B., and Rickard, D. (2008). Nucleic acids bind to nanoparticulate iron (II) monosulphide in aqueous solutions. *Orig. Life Evol. Biosphere* 38 (3), 257–270. doi:10.1007/s11084-008-9132-7

He, J., Tang, J., Zhang, Z., Wang, L., Liu, Q., and Liu, X. (2021). Magnetic ball–milled FeS@biochar as persulfate activator for degradation of tetracycline. *Chem. Eng. J.* 404, 126997. doi:10.1016/j.cej.2020.126997

He, J., Xiao, Y., Tang, J., Chen, H., and Sun, H. (2019). Persulfate activation with sawdust biochar in aqueous solution by enhanced electron donor–transfer effect. *Sci. Total Environ.* 690, 768–777. doi:10.1016/j.scitotenv.2019.07.043

He, M., Li, W., Xie, Z., Yang, S., He, C., Xiong, Z., et al. (2022). Peracetic acid activation by mechanochemically sulfidated zero valent iron for micropollutants degradation: Enhancement mechanism and strategy for extending applicability. *Water Res.* 222, 118887. doi:10.1016/j.watres.2022.118887

Hong, Q., Liu, C., Wang, Z., Li, R., Liang, X., Wang, Y., et al. (2021). Electron transfer enhancing Fe(II)/Fe(III) cycle by sulfur and biochar in magnetic FeS@biochar to active peroxymonosulfate for 2,4–dichlorophenoxyacetic acid degradation. *Chem. Eng. J.* 417, 129238. doi:10.1016/j.cej.2021.129238

Hou, K., Pi, Z., Chen, F., He, L., Yao, F., Chen, S., et al. (2022). Peroxymonosulfate (PMS) activation by mackinawite for the degradation of organic pollutants: Underappreciated role of dissolved sulfur derivatives. *Sci. Total Environ.* 811, 151421. doi:10.1016/j.scitotenv.2021.151421

Hou, K., Pi, Z., Yao, F., Wu, B., He, L., Li, X., et al. (2021). A critical review on the mechanisms of persulfate activation by iron–based materials: Clarifying some ambiguity and controversies. *Chem. Eng. J.* 407, 127078. doi:10.1016/j.cej.2020.127078

Hou, X., Huang, X., Ai, Z., Zhao, J., and Zhang, L. (2016). Ascorbic acid/Fe@Fe_2O_3: A highly efficient combined fenton reagent to remove organic contaminants. *J. Hazard Mater* 310, 170–178. doi:10.1016/j.jhazmat.2016.01.020

Huang, D., He, J., Gu, Y., and He, F. (2017). Mechanochemically sulfidated zero valent iron as an efficient Fenton–like catalyst for degradation of organic contaminants. *Acta Chim. Sin.* 75 (9), 866. doi:10.6023/a17020060

Hussain, I., Li, M., Zhang, Y., Li, Y., Huang, S., Du, X., et al. (2017). Insights into the mechanism of persulfate activation with nZVI/BC nanocomposite for the degradation of nonylphenol. *Chem. Eng. J.* 311, 163–172. doi:10.1016/j.cej.2016.11.085

Jin, Z., Li, Y., Dong, H., Xiao, S., Xiao, J., Chu, D., et al. (2022). A comparative study on the activation of persulfate by mackinawite@biochar and pyrite@biochar for sulfamethazine degradation: The role of different natural iron–sulfur minerals doping. *Chem. Eng. J.* 448, 137620. doi:10.1016/j.cej.2022.137620

Kim, E., Kim, J., Azad, A., and Chang, Y. (2011). Facile synthesis and characterization of Fe/FeS nanoparticles for environmental applications. *Acs Appl. Mater Inter* 3 (5), 1457–1462. doi:10.1021/am200016v

Kong, L., Fang, G., Chen, Y., Xie, M., Zhu, F., Ma, L., et al. (2019). Efficient activation of persulfate decomposition by Cu_2FeSnS_4 nanomaterial for bisphenol A degradation: Kinetics, performance and mechanism studies. *Appl. Catal. B Environ.* 253, 278–285. doi:10.1016/j.apcatb.2019.04.069

Labiadh, L., Oturan, M. A., Panizza, M., Hamadi, N. B., and Ammar, S. (2015). Complete removal of AHPS synthetic dye from water using new electro–fenton oxidation catalyzed by natural pyrite as heterogeneous catalyst. *J. Hazard Mater* 297, 34–41. doi:10.1016/j.jhazmat.2015.04.062

Li, H., Wan, J., Ma, Y., and Wang, Y. (2016). Reaction pathway and oxidation mechanisms of dibutyl phthalate by persulfate activated with zero–valent iron. *Sci. Total Environ.* 562, 889–897. doi:10.1016/j.scitotenv.2016.04.093

Li, J., Liu, Q., Gou, G., Kang, S., Tan, X., Tan, B., et al. (2022c). New insight into the mechanism of peroxymonosulfate activation by Fe_3S_4: Radical and non–radical oxidation. *Sep. Purif. Technol.* 286, 120471. doi:10.1016/j.seppur.2022.120471

Li, J., Ren, Y., Ji, F., and Lai, B. (2017a). Heterogeneous catalytic oxidation for the degradation of p–nitrophenol in aqueous solution by persulfate activated with $CuFe_2O_4$ magnetic nano–particles. *Chem. Eng. J.* 324, 63–73. doi:10.1016/j.cej.2017.04.104

Li, J., Wan, Y., Li, Y., Yao, G., and Lai, B. (2019a). Surface Fe(III)/Fe(II) cycle promoted the degradation of atrazine by peroxymonosulfate activation in the presence of hydroxylamine. *Appl. Catal. B Environ.* 256, 117782. doi:10.1016/j.apcatb.2019.117782

Li, J., Yang, L., Lai, B., Liu, C., He, Y., Yao, G., et al. (2021a). Recent progress on heterogeneous Fe–based materials induced persulfate activation for organics removal. *Chem. Eng. J.* 414, 128674. doi:10.1016/j.cej.2021.128674

Li, J., Zhang, X., Sun, Y., Liang, L., Pan, B., Zhang, W., et al. (2017b). Advances in sulfidation of zerovalent iron for water decontamination. *Environ. Sci. Technol.* 51 (23), 13533–13544. doi:10.1021/acs.est.7b02695

Li, J., Zou, J., Zhang, S., Cai, H., Huang, Y., Lin, J., et al. (2022b). Sodium tetraborate simultaneously enhances the degradation of acetaminophen and reduces the formation potential of chlorinated by–products with heat–activated peroxymonosulfate oxidation. *Water Res.* 224, 119095. doi:10.1016/j.watres.2022.119095

Li, X., Liu, X., Lin, C., Zhang, H., Zhou, Z., Fan, G., et al. (2019b). Activation of peroxymonosulfate by magnetic catalysts derived from drinking water treatment

residuals for the degradation of atrazine. *J. Hazard Mater* 366, 402–412. doi:10.1016/j.jhazmat.2018.12.016

Li, X., Zhou, M., and Pan, Y. (2018). Enhanced degradation of 2,4–dichlorophenoxyacetic acid by pre–magnetization Fe–C activated persulfate: Influential factors, mechanism and degradation pathway. *J. Hazard Mater* 353, 454–465. doi:10.1016/j.jhazmat.2018.04.035

Li, Y., Dong, H., Li, L., Tang, L., Tian, R., Li, R., et al. (2021b). Recent advances in waste water treatment through transition metal sulfides–based advanced oxidation processes. *Water Res.* 192, 116850. doi:10.1016/j.watres.2021.116850

Li, Y., Li, J., Pan, Y., Xiong, Z., Yao, G., Xie, R., et al. (2020). Peroxymonosulfate activation on $FeCo_2S_4$ modified g–C_3N_4 ($FeCo_2S_4$–CN): Mechanism of singlet oxygen evolution for nonradical efficient degradation of sulfamethoxazole. *Chem. Eng. J.* 384, 123361. doi:10.1016/j.cej.2019.123361

Li, Y., Zhao, X., Yan, Y., Yan, J., Pan, Y., Zhang, Y., et al. (2019c). Enhanced sulfamethoxazole degradation by peroxymonosulfate activation with sulfide–modified microscale zero–valent iron (S–mFe^0): Performance, mechanisms, and the role of sulfur species. *Chem. Eng. J.* 376, 121302. doi:10.1016/j.cej.2019.03.178

Li, Y., Zhou, Y., Ni, R., Shang, J., and Cheng, X. (2022a). Degradation of sulfamethazine sodium salt by peroxymonosulfate activated by biochar supported $CoFe_2S_4$: Performance, mechanism and response surface method optimization. *J. Environ. Chem. Eng.* 10 (5), 108059. doi:10.1016/j.jece.2022.108059

Liang, C., Guo, Y., Chien, Y., and Wu, Y. (2010). Oxidative degradation of MTBE by Pyrite–Activated persulfate: Proposed reaction pathways. *Ind. Eng. Chem. Res.* 49 (18), 8858–8864. doi:10.1021/ie100740d

Lin, C., and Wu, M. (2014). UV/$S_2O_8^{2-}$ process for degrading polyvinyl alcohol in aqueous solutions. *Chem. Eng. Process. Process Intensif.* 85, 209–215. doi:10.1016/j.cep.2014.08.012

Liu, H., Yao, J., Wang, L., Wang, X., Qu, R., and Wang, Z. (2019). Effective degradation of fenitrothion by zero–valent iron powder (Fe^0) activated persulfate in aqueous solution: Kinetic study and product identification. *Chem. Eng. J.* 358, 1479–1488. doi:10.1016/j.cej.2018.10.153

Liu, J., Peng, C., and Shi, X. (2022a). Preparation, characterization, and applications of Fe–based catalysts in advanced oxidation processes for organics removal: A review. *Environ. Pollut.* 293, 118565. doi:10.1016/j.envpol.2021.118565

Liu, W., Ai, Z., Cao, M., and Zhang, L. (2014). Ferrous ions promoted aerobic simazine degradation with Fe@Fe_2O_3 core–shell nanowires. *Appl. Catal. B Environ.* 150–151, 1–11. doi:10.1016/j.apcatb.2013.11.034

Liu, W., Wang, Y., Ai, Z., and Zhang, L. (2015). Hydrothermal synthesis of FeS_2 as a High–Efficiency fenton reagent to degrade alachlor via Superoxide–Mediated Fe(II)/Fe(III) cycle. *Acs Appl. Mater Inter* 7 (51), 28534–28544. doi:10.1021/acsami.5b09919

Liu, X., Li, H., Gao, S., Bai, Z., and Tian, J. (2022b). Peroxymonosulfate activation by different iron sulfides for bisphenol–A degradation: Performance and mechanism. *Sep. Purif. Technol.* 289, 120751. doi:10.1016/j.seppur.2022.120751

Luo, T., Feng, H., Tang, L., Lu, Y., Tang, W., Chen, S., et al. (2020). Efficient degradation of tetracycline by heterogeneous electro–Fenton process using Cu–doped Fe@Fe_2O_3: Mechanism and degradation pathway. *Chem. Eng. J.* 382, 122970. doi:10.1016/j.cej.2019.122970

Lyu, H., Gao, B., He, F., Zimmerman, A. R., Ding, C., Tang, J., et al. (2018a). Experimental and modeling investigations of ball–milled biochar for the removal of aqueous methylene blue. *Chem. Eng. J.* 335, 110–119. doi:10.1016/j.cej.2017.10.130

Lyu, H., Tang, J., Shen, B., and Siddique, T. (2018b). Development of a novel chem–bio hybrid process using biochar supported nanoscale iron sulfide composite and Corynebacterium variabile HRJ4 for enhanced trichloroethylene dechlorination. *Water Res.* 147, 132–141. doi:10.1016/j.watres.2018.09.038

Ma, J., Yang, M., Yu, F., and Chen, J. (2015). Easy solid–phase synthesis of pH–insensitive heterogeneous CNTs/FeS Fenton–like catalyst for the removal of antibiotics from aqueous solution. *J. Colloid Interf. Sci.* 444, 24–32. doi:10.1016/j.jcis.2014.12.027

Ma, W., Wang, N., Du, Y., Tong, T., Zhang, L., Andrew Lin, K., et al. (2019). One–step synthesis of novel Fe_3C@nitrogen–doped carbon nanotubes/graphene nanosheets for catalytic degradation of Bisphenol A in the presence of peroxymonosulfate. *Chem. Eng. J.* 356, 1022–1031. doi:10.1016/j.cej.2018.09.093

Ma, Y., Gu, Y., Jiang, D., Mao, X., and Wang, D. (2021). Degradation of 2,4–DCP using persulfate and iron/E–carbon micro–electrolysis coupling system. *J. Hazard Mater* 413, 125381. doi:10.1016/j.jhazmat.2021.125381

Ma, Z., Yang, Y., Jiang, Y., Xi, B., Yang, T., Peng, X., et al. (2017). Enhanced degradation of 2,4–dinitrotoluene in groundwater by persulfate activated using iron–carbon micro–electrolysis. *Chem. Eng. J.* 311, 183–190. doi:10.1016/j.cej.2016.11.083

Mariëtte, W., Sjierk, J. V. D. G., and David, R. (2003). The structure of disordered mackinawite. *Am. Mineral.* 88 (11–12), 2007–2015. doi:10.2138/am-2003-11-1245

Meng, F., Song, M., Song, B., Wei, Y., Cao, Q., and Cao, Y. (2020). Enhanced degradation of Rhodamine B via α–Fe_2O_3 microspheres induced persulfate to generate reactive oxidizing species. *Chemosphere* 243, 125322. doi:10.1016/j.chemosphere.2019.125322

Mohamed, M. M., Abdelmonem, E. E., and El–Sayed, G. O. (2023). Graphene foam mediated FeS_2/α–Fe_2O_3 composites for chloramphenicol photodegradation using persulfate activation under visible light irradiation. *J. Water Process Eng.* 53, 103633. doi:10.1016/j.jwpe.2023.103633

Nair, M. G., Nirmala, M., Rekha, K., and Anukaliani, A. (2011). Structural, optical, photo catalytic and antibacterial activity of ZnO and Co doped ZnO nanoparticles. *Mater Lett.* 65 (12), 1797–1800. doi:10.1016/j.matlet.2011.03.079

Nie, W., Mao, Q., Ding, Y., Hu, Y., and Tang, H. (2019). Highly efficient catalysis of chalcopyrite with surface bonded ferrous species for activation of peroxymonosulfate toward degradation of bisphenol A: A mechanism study. *J. Hazard Mater* 364, 59–68. doi:10.1016/j.jhazmat.2018.09.078

Oh, S., Kang, S., Kim, D., and Chiu, P. C. (2011). Degradation of 2,4–dinitrotoluene by persulfate activated with iron sulfides. *Chem. Eng. J.* 172 (2–3), 641–646. doi:10.1016/j.cej.2011.06.023

Paknikar, K. M., Nagpal, V., Pethkar, A. V., and Rajwade, J. M. (2005). Degradation of lindane from aqueous solutions using iron sulfide nanoparticles stabilized by biopolymers. *Sci. Technol. Adv. Mat.* 6 (3–4), 370–374. doi:10.1016/j.stam.2005.02.016

Pan, Y., Zhou, M., Zhang, Y., Cai, J., Li, B., and Sheng, X. (2018). Enhanced degradation of Rhodamine B by pre–magnetized Fe^0/PS process: Parameters optimization, mechanism and interferences of ions. *Sep. Purif. Technol.* 203, 66–74. doi:10.1016/j.seppur.2018.03.039

Pastor, J., Dewey, B., Johnson, N. W., Swain, E. B., Monson, P., Peters, E. B., et al. (2017). Effects of sulfate and sulfide on the life cycle ofZizania palustris in hydroponic and mesocosm experiments. *Ecol. Appl.* 27 (1), 321–336. doi:10.1002/eap.1452

Peng, J., Zhou, H., Liu, W., Ao, Z., Ji, H., Liu, Y., et al. (2020). Insights into heterogeneous catalytic activation of peroxymonosulfate by natural chalcopyrite: pH–dependent radical generation, degradation pathway and mechanism. *Chem. Eng. J.* 397, 125387. doi:10.1016/j.cej.2020.125387

Petrie, B., Barden, R., and Kasprzyk–Hordern, B. (2015). A review on emerging contaminants in wastewaters and the environment: Current knowledge, understudied areas and recommendations for future monitoring. *Water Res.* 72, 3–27. doi:10.1016/j.watres.2014.08.053

Qi, C., Liu, X., Lin, C., Zhang, X., Ma, J., Tan, H., et al. (2014). Degradation of sulfamethoxazole by microwave–activated persulfate: Kinetics, mechanism and acute toxicity. *Chem. Eng. J.* 249, 6–14. doi:10.1016/j.cej.2014.03.086

Qiu, M., Hu, B., Chen, Z., Yang, H., Zhuang, L., and Wang, X. (2021). Challenges of organic pollutant photocatalysis by biochar–based catalysts. *Biochar* 3 (2), 117–123. doi:10.1007/s42773-021-00098-y

Qiu, M., Liu, L., Ling, Q., Cai, Y., Yu, S., Wang, S., et al. (2022). Biochar for the removal of contaminants from soil and water: A review. *Biochar* 4 (1), 19. doi:10.1007/s42773-022-00146-1

Qu, J., Xu, Y., Zhang, X., Sun, M., Tao, Y., Zhang, X., et al. (2022). Ball milling–assisted preparation of N–doped biochar loaded with ferrous sulfide as persulfate activator for phenol degradation: Multiple active sites–triggered radical/non–radical mechanism. *Appl. Catal. B Environ.* 316, 121639. doi:10.1016/j.apcatb.2022.121639

Quoc, T. N., Nguyen, K. H., Thuy, H. N. T., Tien, N. T. H., Minh, C. T. T., Dao, V., et al. (2021). Feasibility of using sequential sulfurized nanoscale zerovalent Iron–Persulfate process to degrade tetrabromobisphenol A. *J. Nanomater*, 2021: 1–8. doi:10.1155/2021/8053120

Rajajayavel, S. R. C., and Ghoshal, S. (2015). Enhanced reductive dechlorination of trichloroethylene by sulfidated nanoscale zerovalent iron. *Water Res.* 78, 144–153. doi:10.1016/j.watres.2015.04.009

Ren, Y., Lin, L., Ma, J., Yang, J., Feng, J., and Fan, Z. (2015). Sulfate radicals induced from peroxymonosulfate by magnetic ferrospinel MFe_2O_4 (M = Co, Cu, Mn, and Zn) as heterogeneous catalysts in the water. *Appl. Catal. B Environ.* 165, 572–578. doi:10.1016/j.apcatb.2014.10.051

Rickard, D., Hatton, B., Murphy, D. M., Butler, I. B., Oldroyd, A., and Hann, A. (2011). FeS–Induced radical formation and its effect on plasmid DNA. *Aquat. Geochem* 17 (4–5), 545–566. doi:10.1007/s10498-010-9116-x

Savun–Hekimoğlu, B. (2020). A review on sonochemistry and its environmental applications. *Acoustics–Basel* 2 (4), 766–775. doi:10.3390/acoustics2040042

Shang, W., Dong, Z., Li, M., Song, X., Zhang, M., Jiang, C., et al. (2019). Degradation of diatrizoate in water by Fe(II)–activated persulfate oxidation. *Chem. Eng. J.* 361, 1333–1344. doi:10.1016/j.cej.2018.12.139

Shao, D., Ren, X., Wen, J., Hu, S., Xiong, J., Jiang, T., et al. (2016). Immobilization of uranium by biomaterial stabilized FeS nanoparticles: Effects of stabilizer and enrichment mechanism. *J. Hazard Mater* 302, 1–9. doi:10.1016/j.jhazmat.2015.09.043

Shi, Y., Wang, X., Liu, X., Ling, C., Shen, W., and Zhang, L. (2020). Visible light promoted Fe_3S_4 Fenton oxidation of atrazine. *Appl. Catal. B Environ.* 277, 119229. doi:10.1016/j.apcatb.2020.119229

Show, B., Mukherjee, N., and Mondal, A. (2017). Reusable iron sulfide nanospheres towards promoted photocatalytic and electrocatalytic activities. *New J. Chem.* 41 (18), 10083–10095. doi:10.1039/c7nj02018j

Silveira, J. E., Garcia–Costa, A. L., Cardoso, T. O., Zazo, J. A., and Casas, J. A. (2017). Indirect decolorization of azo dye Disperse Blue 3 by electro–activated persulfate. *Electrochim Acta* 258, 927–932. doi:10.1016/j.electacta.2017.11.143

Song, Q., Feng, Y., Wang, Z., Liu, G., and Lv, W. (2019). Degradation of triphenyl phosphate (TPhP) by $CoFe_2O_4$–activated peroxymonosulfate oxidation process: Kinetics, pathways, and mechanisms. *Sci. Total Environ.* 681, 331–338. doi:10.1016/j.scitotenv.2019.05.105

Song, S., Su, Y., Adeleye, A. S., Zhang, Y., and Zhou, X. (2017). Optimal design and characterization of sulfide–modified nanoscale zerovalent iron for diclofenac removal. *Appl. Catal. B Environ.* 201, 211–220. doi:10.1016/j.apcatb.2016.07.055

Soori, M., Zarezadeh, K., Sheibani, S., and Rashchi, F. (2016). Mechano–chemical processing and characterization of nano–structured FeS powder. *Adv. Powder Technol.* 27 (2), 557–563. doi:10.1016/j.apt.2016.02.004

Su, Y., Jassby, D., Song, S., Zhou, X., Zhao, H., Filip, J., et al. (2018). Enhanced oxidative and adsorptive removal of diclofenac in heterogeneous Fenton–like reaction with sulfide modified nanoscale zerovalent iron. *Environ. Sci. Technol.* 52 (11), 6466–6475. doi:10.1021/acs.est.8b00231

Sühnholz, S., Gawel, A., Kopinke, F., and Mackenzie, K. (2021). Evidence of heterogeneous degradation of PFOA by activated persulfate – FeS as adsorber and activator. *Chem. Eng. J.* 423, 130102. doi:10.1016/j.cej.2021.130102

Sühnholz, S., Kopinke, F., and Mackenzie, K. (2022). Heterogeneous activation of persulfate by FeS – surface influence on selectivity. *Chem. Eng. J.* 450, 138192. doi:10.1016/j.cej.2022.138192

Sühnholz, S., Kopinke, F., and Mackenzie, K. (2020). Reagent or catalyst? – FeS as activator for persulfate in water. *Chem. Eng. J.* 387, 123804. doi:10.1016/j.cej.2019.123804

Sun, M., Cheng, G., Ge, X., Chen, M., Wang, C., Lou, L., et al. (2018a). Aqueous Hg(II) immobilization by chitosan stabilized magnetic iron sulfide nanoparticles. *Sci. Total Environ.* 621, 1074–1083. doi:10.1016/j.scitotenv.2017.10.119

Sun, Y., Gu, M., Lyu, S., Brusseau, M. L., Li, M., Lyu, Y., et al. (2020). Efficient removal of trichloroethene in oxidative environment by anchoring nano FeS on reduced graphene oxide supported nZVI catalyst: The role of FeS on oxidant decomposition and iron leakage. *J. Hazard Mater* 392, 122328. doi:10.1016/j.jhazmat.2020.122328

Sun, Y., Liu, Y., Lou, Z., Yang, K., Lv, D., Zhou, J., et al. (2018b). Enhanced performance for Hg(II) removal using biomaterial (CMC/gelatin/starch) stabilized FeS nanoparticles: Stabilization effects and removal mechanism. *Chem. Eng. J.* 344, 616–624. doi:10.1016/j.cej.2018.03.126

Suroshe, J. S., Mlowe, S., Garje, S. S., and Revaprasadu, N. (2018). Preparation of iron sulfide nanomaterials from iron(II) thiosemicarbazone complexes and their application in photodegradation of methylene blue. *J. Inorg. Organomet. P* 28 (3), 603–611. doi:10.1007/s10904-018-0816-9

Tan, C., Dong, Y., Fu, D., Gao, N., Ma, J., and Liu, X. (2018). Chloramphenicol removal by zero valent iron activated peroxymonosulfate system: Kinetics and mechanism of radical generation. *Chem. Eng. J.* 334, 1006–1015. doi:10.1016/j.cej.2017.10.020

Tan, C., Gao, N., Deng, Y., Deng, J., Zhou, S., Li, J., et al. (2014). Radical induced degradation of acetaminophen with Fe3O4 magnetic nanoparticles as heterogeneous activator of peroxymonosulfate. *J. Hazard Mater* 276, 452–460. doi:10.1016/j.jhazmat.2014.05.068

Turcio–Ortega, D., Fan, D., Tratnyek, P. G., Kim, E., and Chang, Y. (2012). Reactivity of Fe/FeS nanoparticles: Electrolyte composition effects on corrosion electrochemistry. *Environ. Sci. Technol.* 46 (22), 12484–12492. doi:10.1021/es303422w

Van Koetsem, F., Van Havere, L., and Du Laing, G. (2016). Impact of carboxymethyl cellulose coating on iron sulphide nanoparticles stability, transport, and mobilization potential of trace metals present in soils and sediment. *J. Environ. Manage* 168, 210–218. doi:10.1016/j.jenvman.2015.10.047

Wang, G., Yang, Y., Xu, X., Zhang, S., Yang, Z., Cheng, Z., et al. (2023b). Rape straw supported FeS nanoparticles with encapsulated structure as peroxymonosulfate and hydrogen peroxide activators for enhanced oxytetracycline degradation. *Molecules* 28 (6), 2771. doi:10.3390/molecules28062771

Wang, J., Liao, Z., Ifthikar, J., Shi, L., Chen, Z., and Chen, Z. (2017). One–step preparation and application of magnetic sludge–derived biochar on acid orange 7 removal via both adsorption and persulfate based oxidation. *Rsc Adv.* 7 (30), 18696–18706. doi:10.1039/c7ra01425b

Wang, J., and Wang, S. (2018). Activation of persulfate (PS) and peroxymonosulfate (PMS) and application for the degradation of emerging contaminants. *Chem. Eng. J.* 334, 1502–1517. doi:10.1016/j.cej.2017.11.059

Wang, J., Xiong, B., Miao, L., Wang, S., Xie, P., Wang, Z., et al. (2021). Applying a novel advanced oxidation process of activated peracetic acid by $CoFe_2O_4$ to efficiently degrade sulfamethoxazole. *Appl. Catal. B Environ.* 280, 119422. doi:10.1016/j.apcatb.2020.119422

Wang, L., Huang, X., Han, M., Lyu, L., Li, T., Gao, Y., et al. (2019). Efficient inhibition of photogenerated electron–hole recombination through persulfate activation and dual–pathway degradation of micropollutants over iron molybdate. *Appl. Catal. B Environ.* 257, 117904. doi:10.1016/j.apcatb.2019.117904

Wang, Q., Tian, S., and Ning, P. (2014). Degradation mechanism of methylene blue in a heterogeneous Fenton–like reaction catalyzed by ferrocene. *Ind. Eng. Chem. Res.* 53 (2), 643–649. doi:10.1021/ie403402q

Wang, X., Wang, Y., Chen, N., Shi, Y., and Zhang, L. (2020c). Pyrite enables persulfate activation for efficient atrazine degradation. *Chemosphere* 244, 125568. doi:10.1016/j.chemosphere.2019.125568

Wang, Y., Gu, Z., Yang, S., and Zhang, A. (2020a). Activation of persulfate by microwave radiation combined with FeS for treatment of wastewater from explosives production. *Environ. Sci. Water Res. Technol.* 6 (3), 581–592. doi:10.1039/c9ew00803a

Wang, Y., Gu, Z., Yang, S., and Zhang, A. (2020b). Performance of a microwave radiation induced persulfate–hydrogen peroxide binary–oxidant process in treating dinitrodiazophenol wastewater. *Sep. Purif. Technol.* 236, 116253. doi:10.1016/j.seppur.2019.116253

Wang, Y., Lin, Y., Yang, C., Wu, S., Fu, X., and Li, X. (2023a). Calcination temperature regulates non–radical pathways of peroxymonosulfate activation via carbon catalysts doped by iron and nitrogen. *Chem. Eng. J.* 451, 138468. doi:10.1016/j.cej.2022.138468

Watson, J. H. P., Croudace, I. W., Warwick, P. E., James, P. A. B., Charnock, J. M., and Ellwood, D. C. (2001). Adsorption of radioactive metals by strongly magnetic iron sulfide nanoparticles produced by sulfate–reducing bacteria. *Sep. Sci. Technol.* 36 (12), 2571–2607. doi:10.1081/ss-100107214

Wei, X., Yuan, H., Li, J., Chen, T., Yuan, Y., Chen, W., et al. (2022). Reactive oxygen species generated in iron sulfide mediated advanced oxidation systems: A critical review of mechanisms and implications for geochemistry and environmental remediation. *J. Environ. Chem. Eng.* 10 (6), 108841. doi:10.1016/j.jece.2022.108841

Wei, Z., Villamena, F. A., and Weavers, L. K. (2017). Kinetics and mechanism of ultrasonic activation of persulfate: An *in situ* EPR spin trapping study. *Environ. Sci. Technol.* 51 (6), 3410–3417. doi:10.1021/acs.est.6b05392

Wharton, M. J., Atkins, B., Charnockab, J. M., Pattrick, R. A. D., and Collison, D. (2000). An X–ray absorption spectroscopy study of the coprecipitation of Tc and Re with mackinawite (FeS). *Appl. Geochem* 15 (3), 347–354. doi:10.1016/s0883-2927(99)00045-1

Wu, J., Wang, B., Cagnetta, G., Huang, J., Wang, Y., Deng, S., et al. (2020a). Nanoscale zero valent iron–activated persulfate coupled with Fenton oxidation process for typical pharmaceuticals and personal care products degradation. *Sep. Purif. Technol.* 239, 116534. doi:10.1016/j.seppur.2020.116534

Wu, J., Wang, X., and Zeng, R. J. (2017). Reactivity enhancement of iron sulfide nanoparticles stabilized by sodium alginate: Taking Cr (VI) removal as an example. *J. Hazard Mater* 333, 275–284. doi:10.1016/j.jhazmat.2017.03.023

Wu, S., Liu, H., Yang, C., Li, X., Lin, Y., Yin, K., et al. (2020b). High–performance porous carbon catalysts doped by iron and nitrogen for degradation of bisphenol F via peroxymonosulfate activation. *Chem. Eng. J.* 392, 123683. doi:10.1016/j.cej.2019.123683

Wu, S., Yang, C., Lin, Y., and Cheng, J. J. (2022). Efficient degradation of tetracycline by singlet oxygen–dominated peroxymonosulfate activation with magnetic nitrogen–doped porous carbon. *J. Environ. Sci.* 115, 330–340. doi:10.1016/j.jes.2021.08.002

Wu, X., Gu, X., Lu, S., Qiu, Z., Sui, Q., Zang, X., et al. (2015). Strong enhancement of trichloroethylene degradation in ferrous ion activated persulfate system by promoting ferric and ferrous ion cycles with hydroxylamine. *Sep. Purif. Technol.* 147, 186–193. doi:10.1016/j.seppur.2015.04.031

Xia, C., Liu, Q., Zhao, L., Wang, L., and Tang, J. (2022). Enhanced degradation of petroleum hydrocarbons in soil by FeS@BC activated persulfate and its mechanism. *Sep. Purif. Technol.* 282, 120060. doi:10.1016/j.seppur.2021.120060

Xiang, W., Chen, H., Zhong, Z., Zhang, C., Lu, X., Huang, M., et al. (2022). Efficient degradation of carbamazepine in a neutral sonochemical FeS/persulfate system based on the enhanced heterogeneous–homogeneous sulfur–iron cycle. *Sep. Purif. Technol.* 282, 120041. doi:10.1016/j.seppur.2021.120041

Xiang, W., Huang, M., Wang, Y., Wu, X., Zhang, F., Li, D., et al. (2020). New insight in the O2 activation by nano Fe/Cu bimetals: The synergistic role of Cu(0) and Fe(II). *Chin. Chem. Lett.* 31 (10), 2831–2834. doi:10.1016/j.cclet.2020.08.006

Xie, Y. F., Li, X. D., and Li, F. D. (2013). Study on application of biological iron sulfide composites in treating vanadium–extraction wastewater containing chromium (VI) and chromium reclamation. *J. Environ. Biol.* 34 (2), 301–305.

Xiong, Z., He, F., Zhao, D., and Barnett, M. O. (2009). Immobilization of mercury in sediment using stabilized iron sulfide nanoparticles. *Water Res.* 43 (20), 5171–5179. doi:10.1016/j.watres.2009.08.018

Xu, H., and Sheng, Y. (2021). New insights into the degradation of chloramphenicol and fluoroquinolone antibiotics by peroxymonosulfate activated with FeS: Performance and mechanism. *Chem. Eng. J.* 414, 128823. doi:10.1016/j.cej.2021.128823

Xu, J., Wang, Y., Weng, C., Bai, W., Jiao, Y., Kaegi, R., et al. (2019). Reactivity, selectivity, and Long–Term performance of sulfidized nanoscale zerovalent iron with different properties. *Environ. Sci. Technol.* 53 (10), 5936–5945. doi:10.1021/acs.est.9b00511

Xu, L., Li, L., Fang, P., Chang, K., Chen, C., and Liao, Q. (2022). Removal of uranium (VI) ions from aqueous solution by graphitic carbon nitride stabilized FeS nanoparticles. *J. Mol. Liq.* 345, 117050. doi:10.1016/j.molliq.2021.117050

Yan, S., Luo, S., Feng, J., Li, P., Guo, R., Wang, Q., et al. (2020). Rational design of flower–like $FeCo_2S_4$/reduced graphene oxide films: Novel binder–free electrodes with ultra–high conductivity flexible substrate for high–performance all–solid–state pseudocapacitor. *Chem. Eng. J.* 381, 122695. doi:10.1016/j.cej.2019.122695

Yan, Z., Gu, Y., Wang, X., Hu, Y., and Li, X. (2021). Degradation of aniline by ferrous ions activated persulfate: Impacts, mechanisms, and by–products. *Chemosphere* 268, 129237. doi:10.1016/j.chemosphere.2020.129237

Yang, S., He, C., Xie, Z., Li, L., Xiong, Z., Zhang, H., et al. (2022). Efficient activation of PAA by FeS for fast removal of pharmaceuticals: The dual role of sulfur species in regulating the reactive oxidized species. *Water Res.* 217, 118402. doi:10.1016/j.watres.2022.118402

Yangju, L., Xiuge, Z., Yan, Y., Jianfei, Y., Yuting, P., Yunhong, Z., et al. (2019). Enhanced sulfamethoxazole degradation by peroxymonosulfate activation with sulfide–modified microscale zero–valent iron (S–mFe^0): Performance, mechanisms, and the role of sulfur species. *Chem. Eng. J.* 376 (C), 121302. doi:10.1016/j.cej.2019.03.178

Ye, Z., Padilla, J. A., Xuriguera, E., Beltran, J. L., Alcaide, F., Brillas, E., et al. (2020). A highly stable metal–organic Framework–Engineered FeS_2/C nanocatalyst for heterogeneous Electro–Fenton treatment: Validation in wastewater at mild pH. *Environ. Sci. Technol.* 54 (7), 4664–4674. doi:10.1021/acs.est.9b07604

Yu, Z., Ma, J., Huang, X., Lv, Y., Liu, Y., Lin, C., et al. (2022). Insights into enhanced peroxydisulfate activation with S doped Fe@C catalyst for the rapid degradation of organic pollutants. *J. Colloid Interf. Sci.* 610, 24–34. doi:10.1016/j.jcis.2021.12.046

Yuan, Y., Tao, H., Fan, J., and Ma, L. (2015). Degradation of p–chloroaniline by persulfate activated with ferrous sulfide ore particles. *Chem. Eng. J.* 268, 38–46. doi:10.1016/j.cej.2014.12.092

Zhang, J., Qiu, S., Feng, H., Hu, T., Wu, Y., Luo, T., et al. (2022). Efficient degradation of tetracycline using core–shell Fe@Fe_2O_3–CeO_2 composite as novel heterogeneous electro–Fenton catalyst. *Chem. Eng. J.* 428, 131403. doi:10.1016/j.cej.2021.131403

Zhang, P., Tan, X., Liu, S., Liu, Y., Zeng, G., Ye, S., et al. (2019a). Catalytic degradation of estrogen by persulfate activated with iron–doped graphitic biochar: Process variables effects and matrix effects. *Chem. Eng. J.* 378 (2), 122141. doi:10.1016/j.cej.2019.122141

Zhang, S., Lyu, H., Tang, J., Song, B., Zhen, M., and Liu, X. (2019b). A novel biochar supported CMC stabilized nano zero–valent iron composite for hexavalent chromium removal from water. *Chemosphere* 217, 686–694. doi:10.1016/j.chemosphere.2018.11.040

Zhang, W., Gao, J., Duan, W., Zhang, D., Jia, J., and Wang, Y. (2020). Sulfidated nanoscale zero–valent iron is an efficient material for the removal and regrowth inhibition of antibiotic resistance genes. *Environ. Pollut.* 263, 114508. doi:10.1016/j.envpol.2020.114508

Zhao, L., Ji, Y., Kong, D., Lu, J., Zhou, Q., and Yin, X. (2016). Simultaneous removal of bisphenol A and phosphate in zero–valent iron activated persulfate oxidation process. *Chem. Eng. J.* 303, 458–466. doi:10.1016/j.cej.2016.06.016

Zhao, Z., Pan, S., Ye, Y., Zhang, X., and Pan, B. (2020). FeS_2/H_2O_2 mediated water decontamination from p–arsanilic acid via coupling oxidation,adsorption and coagulation: Performance and mechanism. *Chem. Eng. J.* 381 (2), 122667. doi:10.1016/j.cej.2019.122667

Zheng, M., Lu, J., and Zhao, D. (2018). Toxicity and transcriptome sequencing (RNA–seq) analyses of adult zebrafish in response to exposure carboxymethyl cellulose stabilized iron sulfide nanoparticles. *Sci. Rep–Uk* 8 (1), 8083. doi:10.1038/s41598-018-26499-x

Zhou, L., Liu, J., and Dong, F. (2017). Spectroscopic study on biological mackinawite (FeS) synthesized by ferric reducing bacteria (FRB) and sulfate reducing bacteria (SRB): Implications for in–situ remediation of acid mine drainage. *Spectrochimica Acta Part A Mol. Biomol. Spectrosc.* 173, 544–548. doi:10.1016/j.saa.2016.09.053

Zhou, X., Luo, M., Xie, C., Wang, H., Wang, J., Chen, Z., et al. (2021a). Tunable S doping from Co_3O_4 to Co_9S_8 for peroxymonosulfate activation: Distinguished Radical/Nonradical species and generation pathways. *Appl. Catal. B Environ.* 282, 119605. doi:10.1016/j.apcatb.2020.119605

Zhou, X., Zeng, Z., Zeng, G., Lai, C., Xiao, R., Liu, S., et al. (2020). Insight into the mechanism of persulfate activated by bone char: Unraveling the role of functional structure of biochar. *Chem. Eng. J.* 401, 126127. doi:10.1016/j.cej.2020.126127

Zhou, Y., Wang, X., Zhu, C., Dionysiou, D. D., Zhao, G., Fang, G., et al. (2018). New insight into the mechanism of peroxymonosulfate activation by sulfur–containing minerals: Role of sulfur conversion in sulfate radical generation. *Water Res.* 142, 208–216. doi:10.1016/j.watres.2018.06.002

Zhou, Z., Huang, J., Xu, Z., Ali, M., Shan, A., Fu, R., et al. (2021b). Mechanism of contaminants degradation in aqueous solution by persulfate in different Fe(II)–based synergistic activation environments: Taking chlorinated organic compounds and benzene series as the targets. *Sep. Purif. Technol.* 273, 118990. doi:10.1016/j.seppur.2021.118990

Zhu, K., Xu, H., Chen, C., Ren, X., Alsaedi, A., and Hayat, T. (2019). Encapsulation of Fe^0–dominated Fe_3O_4/Fe^0/Fe_3C nanoparticles into carbonized polydopamine nanospheres for catalytic degradation of tetracycline via persulfate activation. *Chem. Eng. J.* 372, 304–311. doi:10.1016/j.cej.2019.04.157

Zhuang, Y., Wang, X., Zhang, L., Dionysiou, D. D., Kou, Z., and Shi, B. (2020). Double–network hydrogel templated FeS/graphene with enhanced PMS activation performance: Considering the effect of the template and iron species. *Environ. Sci. Nano* 7 (3), 817–828. doi:10.1039/c9en01391a